The Plant Cell, Vol. 18, 3015–3032, November 2006, www.plantcell.org © 2006 American Society of Plant Biologists

Wax-deficient anther1 Is Involved in Cuticle and Wax Production in Rice Anther Walls and Is Required for Pollen Development [W]

Ki-Hong Jung,[a,1] Min-Jung Han,[a] Dong-yeun Lee,[a] Yang-Seok Lee,[a] Lukas Schreiber,[b] Rochus Franke,[b] Andrea Faust,[c] Alexander Yephremov,[c] Heinz Saedler,[c] Yong-Woo Kim,[d] Inhwan Hwang,[d] and Gynheung An[a,e,2]

[a] National Research Laboratory of Plant Functional Genomics, Division of Molecular and Life Sciences, Pohang University of Science and Technology, Pohang 790-784, Republic of Korea
[b] Institute of Cellular and Molecular Botany, University of Bonn, D-53115 Bonn, Germany
[c] Department of Molecular Genetics, Max Planck Institute for Breeding Research, D-50829 Köln, Germany
[d] Center for Plant Intracellular Trafficking and Division of Molecular and Life Sciences, Pohang University of Science and Technology, Pohang 790-784, Republic of Korea
[e] Functional Genomic Center, Pohang University of Science and Technology, Pohang 790-784, Republic of Korea

In vegetative leaf tissues, cuticles including cuticular waxes are important for protection against nonstomatal water loss and pathogen infection as well as for adaptations to environmental stress. However, their roles in the anther wall are rarely studied. The innermost layer of the anther wall (the tapetum) is essential for generating male gametes. Here, we report the characterization of a T-DNA insertional mutant in the *Wax-deficient anther1* (*Wda1*) gene of rice (*Oryza sativa*), which shows significant defects in the biosynthesis of very-long-chain fatty acids in both layers. This gene is strongly expressed in the epidermal cells of anthers. Scanning electron microscopy analyses showed that epicuticular wax crystals were absent in the outer layer of the anther and that microspore development was severely retarded and finally disrupted as a result of defective pollen exine formation in the mutant anthers. These biochemical and developmental defects in tapetum found in *wda1* mutants are earlier events than those in other male-sterile mutants, which showed defects of lipidic molecules in exine. Our findings provide new insights into the biochemical and developmental aspects of the role of waxes in microspore exine development in the tapetum as well as the role of epicuticular waxes in anther expansion.

INTRODUCTION

Waxes are major constituents of the cuticle, a hydrophobic barrier covering the aerial portions of land plants. The primary role of epicuticular waxes is protection from water loss (Riederer and Schreiber, 2001), but they are also believed to play important roles in plant defenses against bacterial and fungal pathogens (Jenks et al., 1994). Plant waxes predominantly comprise alcohols, aldehydes, ketones, alkanes, and esters derived from very-long-chain fatty acids (VLCFAs), ranging in chain length from C20 to C34 (Kunst and Samuels, 2003). Core biosynthetic activities to extend the acyl chain to the desired length are the sequential extensions performed by fatty acid elongation (FAE) complexes, involving four enzymatic reactions. Several rate-limiting FAE condensing enzymes exist, including β-KETO ACYL-COA SYNTHASE1 (KCS1), ECERIFERUM6 (CER6), FIDDLEHEAD, and Le CER6, which have been implicated in wax biosynthesis (Todd et al., 1999; Fiebig et al., 2000; Pruitt et al., 2000; Vogg et al., 2004). Molecular characterization of the maize (*Zea mays*) *glossy8* (*gl8*) mutant has resulted in the identification of another component of the FAE complex, which catalyzes 3-ketoacyl reductase reaction (Xu et al., 1997, 2002; Dietrich et al., 2005). Disruption of the *Arabidopsis thaliana Enoyl-CoA reductase* (*ECR*) gene, which is another FAE component, causes a reduction in the cuticle wax load (Zheng et al., 2005). VLCFAs are converted to other wax components through either an acyl reduction pathway or a decarbonylation pathway. The former gives rise to primary alcohols and wax esters, and the latter leads to the formation of aldehydes, alkanes, secondary alcohols, and ketones (Millar et al., 1999; Kunst and Samuels, 2003). In the garden pea (*Pisum sativum*), alcohol formation from VLCFA precursors is performed by FATTY ACYL-COA REDUCTASE (FAR) (Vioque and Kolattukudy, 1997). The FAR-related *Arabidopsis* gene, *MALE STERILITY2* (*MS2*), encodes a tapetum-specific protein essential for pollen fertility (Aarts et al., 1997). Biochemical studies of TRITICUM AESTIVUM ANTHER1, a wheat (*Triticum aestivum*) anther-specific homolog, supports the notion that MS2 might act as a FAR in the formation of fatty alcohols required for wax ester production in the tapetum (Wang et al., 2002).

Stem wax analysis of the *cer1* mutant has shown a strong reduction in products of the decarbonylation pathway (e.g.,

[1] Current address: Department of Plant Pathology, University of California Davis, Davis, CA 95616.
[2] To whom correspondence should be addressed. E-mail genean@postech.ac.kr; fax 82-54-279-0659.
The author responsible for distribution of materials integral to the findings presented in this article in accordance with the policy described in the Instructions for Authors (www.plantcell.org) is: Gynheung An (genean@postech.ac.kr).
[W] Online version contains Web-only data.
www.plantcell.org/cgi/doi/10.1105/tpc.106.042044

alkanes, secondary alcohols, and ketones) accompanied by an increase in aldehydes (Aarts et al., 1995). CER1 shares considerable sequence similarity with maize GL1, which is proposed to be a membrane-bound protein affecting wax biosynthesis (Hansen et al., 1997). CER1 and GL1 appear to perform a different role in cuticular wax biosynthesis. Further work is needed to resolve the functional identities of these proteins.

Cuticular waxes are embedded and overlaid on a polyester matrix of cutin (Nawrath, 2003). The combination of cutin, waxes, and possibly polysaccharides forms the cuticle (Jeffree, 1996; Kolattukudy, 1996). Cutin plays an important role in protecting organisms from water loss, UV irradiation, frost damage, and attacks from pathogens and insects. Cutin is predominantly built from C16 and C18 aliphatics, typically ester-linked via carboxy and ω-hydroxy groups of individual fatty acid derivatives. These monomers frequently contain additional hydroxyl and epoxy groups in the midchain positions. Although a biosynthesis pathway of cutin monomers has been proposed, based on the analysis of the cutin composition of cell surfaces fed with radiolabeled cutin monomer precursors, very little is known about this unique plant process (Kolattukudy, 1996).

In angiosperm species, the anther wall has four layers: outermost epidermis, endothecium, middle layer, and innermost tapetum. Whereas the epidermis is important in protecting an organism from various environmental stresses and pathogen attacks, the tapetum plays a critical role in pollen development and maturation. Pollen grains are covered by lipid-derived structures that are essential for pollen dispersal, pollen–stigma communication, and pollen rehydration (Piffanelli et al., 1997, 1998). The pollen wall comprises three layers: pollen coat, outer exine layer, and inner intine layer. The highly sculpted outer layer exine is largely composed of sporopollenin, which is resistant to degradation and withstands acetolysis (Scott, 1994). Sporopollenin is made up of polymers derived from VLCFAs and their derivatives plus more modest amounts of oxygenated aromatic rings and phenylpropanoids (Guilford et al., 1988; Wehling et al., 1989; Wiermann and Gubatz, 1992; Wilmesmeier et al., 1993; Ahlers et al., 1999; Meuter-Gerhards et al., 1999).

Functional and biochemical roles of the exine have been studied using mutants defective in pollen wall development and exine deposition, such as *defective in exine formation1* (*dex1*), *ms2*, *no exine formation1*, *faceless pollen1*, and *cer6* mutants in *Arabidopsis* (Aarts et al., 1997; Fiebig et al., 2000; Paxson-Sowders et al., 2001; Ariizumi et al., 2003, 2004; Kunst and Samuels, 2003). In cereal crops, wheat and rice (*Oryza sativa*) RAFTIN proteins are localized at orbicule and exine and are essential for the maturation process of pollen development, but their biochemical characteristics have not been determined (Wang et al., 2003).

Here, we describe a male-sterile mutant of rice, *wax-deficient anther1* (*wda1*), that was generated through T-DNA insertional mutation (Jeon et al., 2000; Jung et al., 2003, 2005; Lee et al., 2003, 2004). This mutant shows morphological changes in its pollen and anther walls as well as alterations in its wax composition. *Wda1* encodes a protein with high similarity to proteins involved in wax production (Aarts et al., 1995; Hansen et al., 1997; Chen et al., 2003). Our biochemical analysis of the *wda1* anthers demonstrated that the levels of very-long-chain alkanes, alkenes, fatty acids, and primary alcohols are severely reduced in mutant anthers. This study revealed the role of VLCFAs in the development of the tapetum and the epidermal layer in the anther wall.

RESULTS

Isolation of a Male-Sterile Mutant from T-DNA–Tagged Lines

We previously reported the generation of T-DNA insertional lines in Japonica rice (Jeong et al., 2002; Jung et al., 2003, 2005). The T-DNA contains a *β-glucuronidase* (*GUS*) reporter gene next to the T-DNA border. Its insertion within a gene can generate a fusion between the *GUS* reporter gene and an endogenous target gene. This feature allows us to identify a group of genes that are expressed in a particular tissue or organ. Among the 270 lines that show GUS activity in their anthers, 15 manifest male-sterile phenotypes that cosegregate with GUS (Jung et al., 2005).

Here, we report the detailed analysis of line 0-208-29. In the T2 progeny, the GUS-positive:GUS-negative ratio was 3:1. Although approximately two-thirds of the GUS-positive plants were fertile, the remaining one-third were sterile as a result of the lack of mature pollen grains. All of the GUS-negative plants were normal. T3 progeny from the GUS-positive fertile plants had the same 3:1 ratio, again, with one-third of the GUS-positive plants being male-sterile (Figure 1A). The mutant anthers were small and white because they lacked mature pollen grains (Figure 1B). This sterile phenotype segregated as a single recessive allele (fertile:sterile = 142:49; $\chi^2 = 0.02$ for 3:1) (Figures 1A and 1B). We named this mutant *wax-deficient anther1* (*wda1*).

Identification of a T-DNA Insertional Mutation in the *Wda1* Gene

To isolate the flanking sequence of the T-DNA, inverse PCR was performed as described previously (Triglia et al., 1988; Jung et al., 2003). Sequence analysis of the T-DNA flanking region of the male-sterile line revealed that the T-DNA is inserted into a gene located on chromosome 10 in the BAC OSJNBa0079L16. Its full-length cDNA was identified as AK100751 in the KOME (for Knowledge-Based Oryza Molecular Biological Encyclopedia) rice full-length cDNA database (http://cdna01.dna.affrc.go.jp/cDNA). The transcript of the tagged gene is 2337 bp long, including an 1866-bp coding sequence. The locus name of this gene has been registered as OSJNBa0079L16.17 in GenBank (http://www.ncbi.nlm.nih.gov) and as LOC_Os10g33250 in The Institute for Genomic Research database (http://tigrblast.tigr.org/euk-blast/). The primary structure of the gene comprises 10 exons and 9 introns (Figure 2A). The T-DNA insertion was located at 311 bp downstream from the ATG start codon, in the first intron of the gene (Figure 2A).

The predicted protein encoded by the tagged gene contains 621 amino acid residues with a molecular mass of 71.2 kD and a pI of 8.24. The protein has 60% identity with rice LOC_Os02g40780, which is the most similar ortholog to *Arabidopsis* CER1, 56% with the *Arabidopsis* CER1 protein (accession number

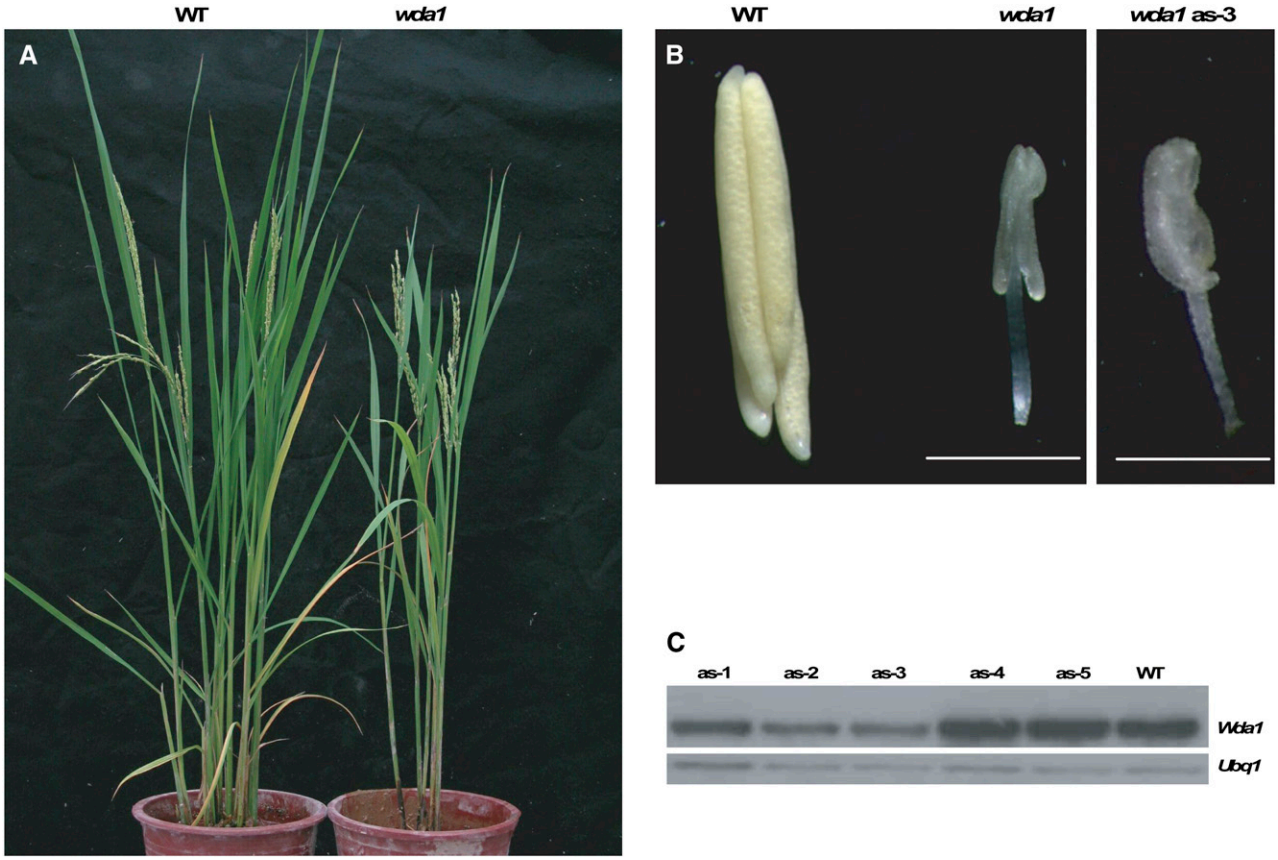

Figure 1. Phenotypes of Wild-Type, *wda1* Knockout, and *Wda1* Underexpressed Plants.

(A) Comparison of wild-type (left) and *wda1* knockout (right) plants after bolting.
(B) Comparison among wild-type (left), *wda1* (middle), and *wda1* as-3 (right) anthers at the pollen mitosis stage. Bars = 1 mm.
(C) Transcript levels of *Wda1* antisense plants. *Wda1* transcript levels were examined by semiquantitative RT-PCR using p3 and p4 primers (see Figure 2A). *Ubiquitin extension protein1* (*Ubq1*) was used as a control. as-1, partial fertile plant; as-2 and as-3, sterile plants; as-4 and as-5, fertile plants; WT, wild-type plant.

BAA11024), 51% with the *Arabidopsis* CER1-like protein (accession number CAA65199), 51% with rice LOC_Os02g56920, and 34% with maize GL1 (accession number AY505017).

Multiple alignments were performed for the seven plant proteins with high similarity to the WDA1 protein (Figure 2B). A functional-domain analysis with Pfam 7.0 (http://www.sanger.ac.uk/Software/Pfam) indicated that the region between the 40th and 258th amino acid residues forms the sterol desaturase domain (gray lines in Figure 2B), which is present in C-5 sterol desaturase and C-4 sterol methyl oxidase. Members containing this conserved region are involved in the biosynthesis of plant cuticular waxes (Aarts et al., 1995; Chen et al., 2003). The prediction of a signal peptide with SignalP 3.0 (http://www.cbs.dtu.dk/services/SignalP/) and PSORT (http://psort.nibb.ac.jp/form.html) suggests that WDA1 comprises a membrane-targeting signal at the N terminus and a putative cleavage site between the 31st and 32nd amino acids. Amino acid sequence analysis using the DAS Transmembrane Prediction server (http://www.sbc.su.se/~miklos/DAS/) classified WDA1 as an integral membrane protein containing five transmembrane domains in the N-terminal region. The WDA1 protein has one His-rich motif, HX3HH, starting at the 146th amino acid plus two HX2HH motifs beginning at positions 157 and 252 in the deduced amino acid sequence (black lines in Figure 2B). Taton et al. (2000) have demonstrated by site-directed mutagenesis that the His residues in His-rich motifs are essential for the catalysis of sterol desaturases, and they proposed that the ligands are divalent metal ions.

Phylogenic analysis of the 14 proteins with high similarities to WDA1 showed that they can be grouped into two clades (Figure 2C). WDA1 groups with CER1 and CER1-like proteins, whereas the WAX2-like proteins form the second clade (Chen et al., 2003). Three rice proteins (LOC_Os02g08230, LOC_Os06g44300, and LOC_Os09g25850) belong to the second clade. *Arabidopsis* CER1 functions in the biosynthesis of stem wax and pollen coat tryphine alkanes (Aarts et al., 1995). The *Arabidopsis* CER1-like protein (accession number CAA65199) is a flower-preferential isozyme of CER1, but its functional defects have not been identified (Aarts et al., 1995). Our phylogenic analysis suggests that WDA1 is likely involved in VLCFA metabolism.

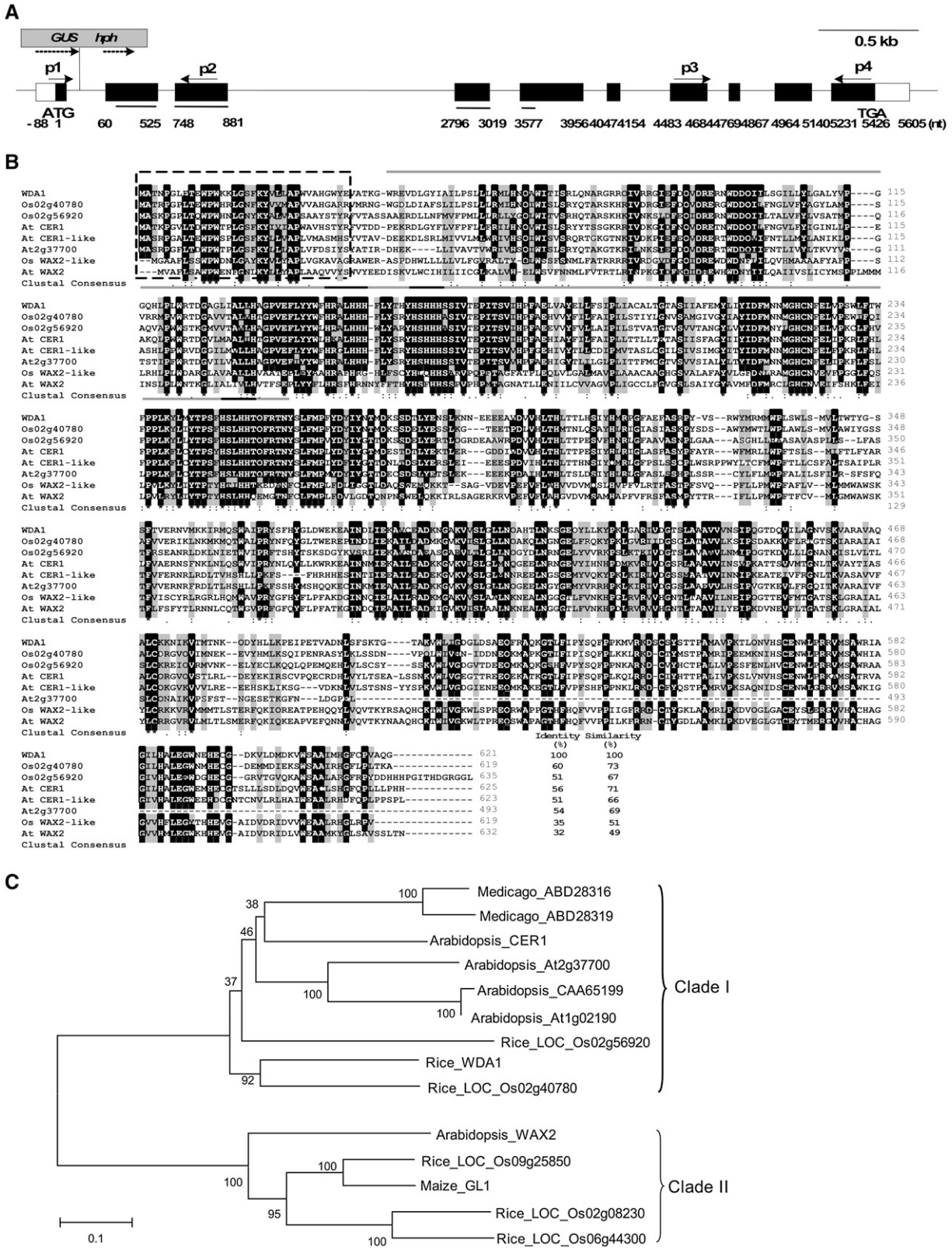

Figure 2. Scheme of the *Wda1* Gene, Multiple Alignments, and Phylogenic Analysis of WDA1-Related Proteins.

(A) *Wda1* gene and relative insertion position of the T-DNA. Closed boxes represent exons, and connecting lines represent introns. The ATG start codon

Downregulation of *Wda1* Causes Male Sterility

To confirm whether the male-sterile phenotype was attributable to mutation in the *Wda1* gene, we generated transgenic plants that underexpressed *Wda1*. The 653-bp N-terminal region of the *Wda1* cDNA was amplified by the p1 and p2 primers (Figure 2A), and the PCR product was placed under the control of the maize ubiquitin promoter in the antisense direction. The construct was introduced into rice calli by the *Agrobacterium tumefaciens*–mediated transformation method (Lee et al., 1999). Among the 74 transgenic plants that grew to maturity, 17 were completely sterile and 32 showed partial fertility. The remaining plants were of normal fertility. RT-PCR analysis of *Wda1* transcript levels in the transgenic plants demonstrated that the fertile lines (as-4 and as-5 in Figure 1C) contained significant amounts of transcript, whereas the sterile lines (as-2 and as-3 in Figures 1B and 1C) contained low levels. The partial sterile line (as-1 in Figure 1C) contained an intermediate amount. Close examination of the *Wda1* as-3 antisense plants revealed small anthers and defective pollen grains, as had been observed with the *wda1* knockout anthers (Figure 1B). These experiments confirmed that mutations in *Wda1* cause anther defects and male-sterile phenotypes.

Wda1 Transcript Is Abundant during Flowering Stages

Because the *GUS* gene located in T-DNA was fused to *Wda1*, the level and pattern of expression of the fusion gene could be assayed for GUS activity. High levels of GUS activity were observed in spikelets from the premeiosis stage to the heading stage (Figures 3A and 3K). GUS activity was also prominent in the outer and inner epidermis (Figure 3H) and trichomes (Figure 3G) of the palea/lemma, lodicules (Figures 3C, 3E, 3F, and 3I), stigmas (Figure 3C), and anthers (Figures 3C, 3D, 3I, and 3J). Cross sections of heterozygotic anthers at the vacuolated pollen stage revealed that GUS was expressed strongly in the epidermis but only weakly in the tapetum, endothecium, and connective tissue (Figure 3J). In vegetative tissue, GUS activity was mostly absent except at collar regions (between the leaf sheath and the leaf blade) and the base of shoots (see Supplemental Figure 1 online).

To examine whether GUS activity truly represented *Wda1* expression patterns, we performed semiquantitative RT-PCR analyses. *Wda1* was highly expressed in panicles at various developmental stages (Figure 3K) but only very weakly in the roots and shoots of 7-d-old seedlings. Only low transcript levels were detected in the developing seeds and flag leaves. In developing spikelets, transcript was detected in all floral organs (Figures 3K and 3L), but it was barely detectable in the *wda1* anthers (Figure 3L). LOC_Os02g40780, which is the most similar rice gene to *Wda1*, was also expressed throughout panicle development. However, its expression was much higher in the shoots and flag leaves. In mature spikelets, transcript levels were low in the anthers and palea/lemma and barely detectable in the ovaries and lodicules (Figure 3L). These results indicate that *Wda1* functions primarily in the panicles, especially in the reproductive organs, whereas LOC_Os02g40780 may play roles in both vegetative and reproductive organs.

Characterization of *wda1* Mutants

To further characterize the phenotypic alterations of mutant anthers, we performed thin-section analyses for wild-type and *wda1* anthers and delineated anther development into six stages based on stages of pollen formation (Figure 4). During the premeiosis stage (Figure 4A), the archespores divided into secondary parietal cells and sporogenous cells. Then, those secondary cells divided into inner (tapetal) layer cells and middle layer cells. In the *wda1* anthers, their sporogenous cells, endothecium, middle layer, and inner layer appeared normal at premeiosis (Figure 4G).

During the meiosis stage (Figure 4B), the sporogenous cells developed into pollen mother cells, which underwent meiosis to form tetrads of haploid microspores. Intine formation of microspores was initiated during late meiosis (see Supplemental Figure 2 online). The outer wall of the anther epidermis consisted of a 60- to 75-nm electron-opaque cuticular membrane on top of the cell wall and an ultrathin second layer covering the principal cuticular membrane (Figure 5Q). The tapetal cells then differentiated and the middle layer cells started to degenerate (Figures 4B and 5B). In *wda1* anthers, the meiocytes were slightly

Figure 2. (continued).

andTGA stop codon are indicated. The insertion position of the T-DNA in line 0-208-29 (gray box) is indicated in the first intron of *Wda1*. The number 1 indicates the starting nucleotide of translation; −88 indicates the starting point of the 5′ untranslated region located 88 bp upstream from ATG; 5426 indicates the genomic nucleotide length from ATG to TGA; and 5605 indicates the end point of the 3′ untranslated region located downstream at 5605 bp from ATG. Numbers represent start and end points of each exon. p1 and p2 are primers for the construction of *Wda1* underexpressed plants, and p3 and p4 are primers for semiquantitative RT-PCR analysis of the *Wda1* transcript. *GUS*, β-glucuronidase; *hph*, hygromycin resistance marker for the selection of T-DNA insertion; nt, nucleotides. Bar = 0.5 kb.

(B) Multiple alignments of plant proteins showing high similarity with the WDA1 protein. WDA1 (top line) was aligned with three rice proteins (LOC_Os02g56920, LOC_Os02g40780, and Os Wax2-like [LOC_Os09g25850]) and four *Arabidopsis* proteins (CER1, CER1-like, At2g37700, and WAX2). Black background indicates amino acid residues that are >70% conserved, and gray background indicates amino acids that are >30% conserved. Asterisks indicate perfectly matched amino acids, colons indicate highly conserved amino acids, and dots indicate low-matched amino acids among these eight proteins. The identity and similarity of the aligned proteins for WDA1 are shown at the end of the alignments. The dotted box indicates transient signal peptides for membrane targeting; the three black lines indicate His-rich motifs (HX3HH) for putative zinc binding; and the gray line indicates a desaturase domain.

(C) Phylogenic analysis of proteins similar to WDA1. Phylogenic analysis by MEGA 2.0 was performed using the neighbor-joining tree with 1000 replicates; the handling gap option was pair-wise deletion. Multiple alignments used for this analysis are shown in Supplemental Table 5 online.

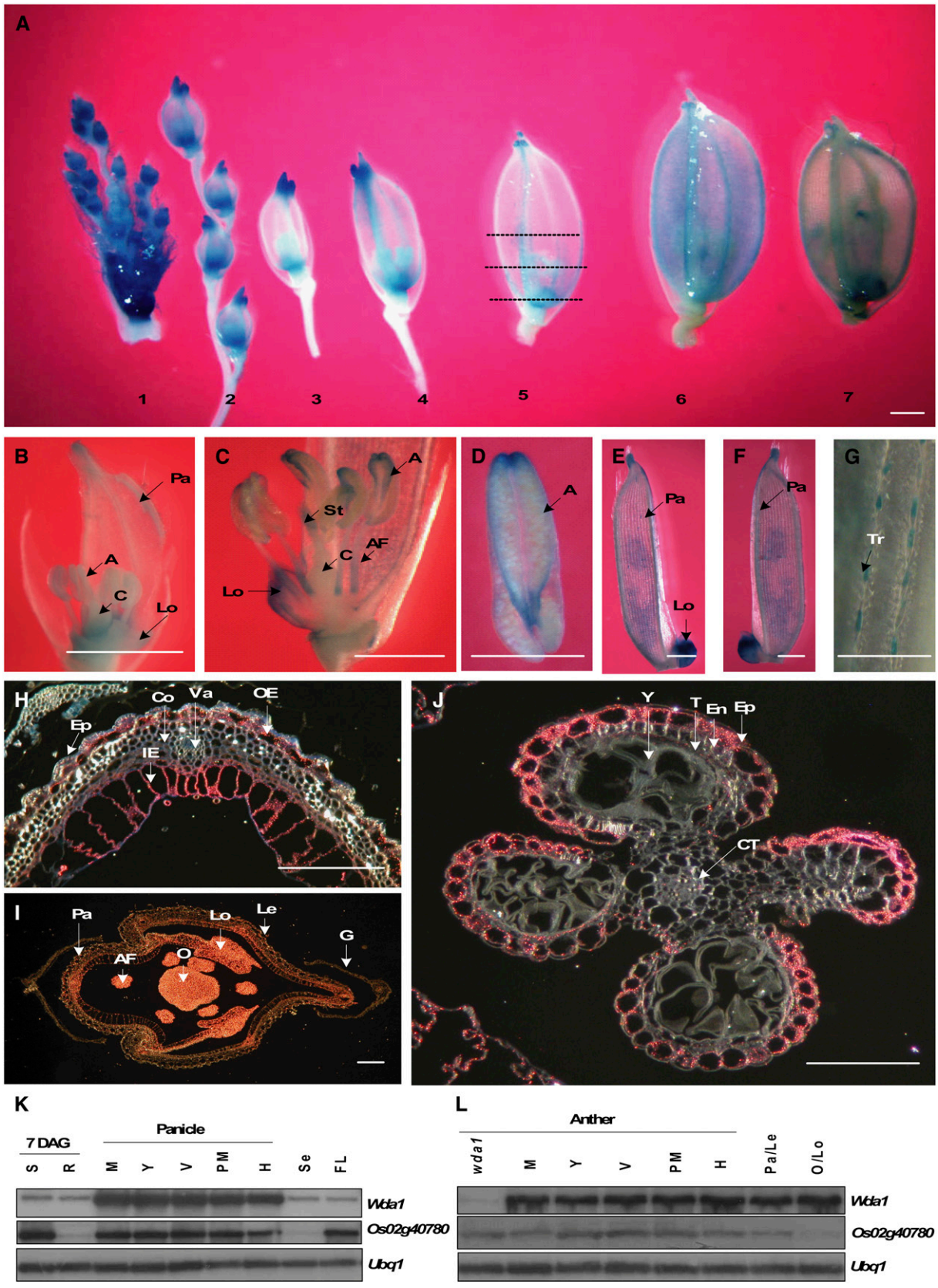

Figure 3. Expression Profiles of *Wda1* by GUS Assay and RT-PCR.

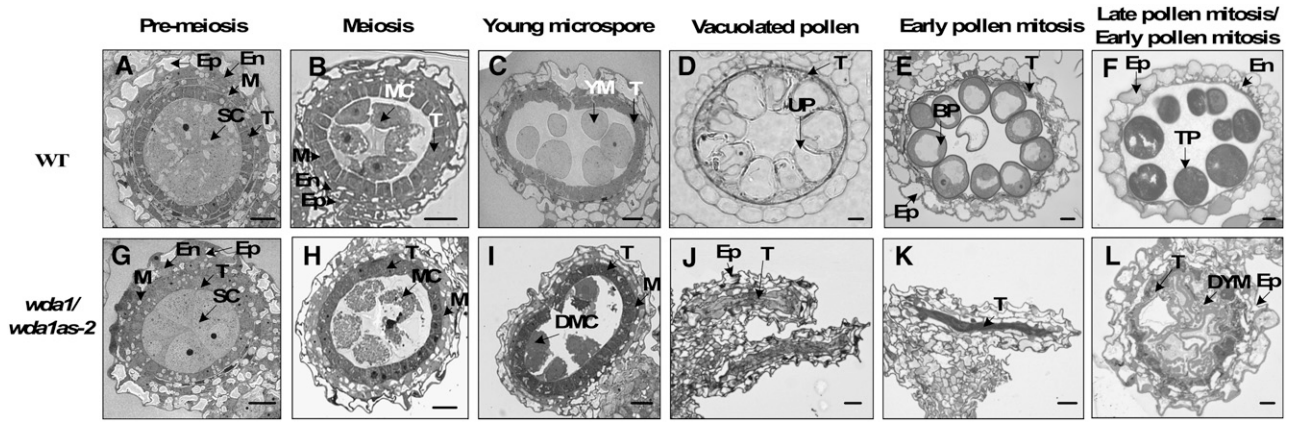

Figure 4. Light Microscopic Analyses of Developing Anthers.

Cross sections of wild-type (**[A]** to **[F]**) and *wda1* (**[G]** to **[K]**) anthers at premeiotic stage (**[A]** and **[G]**), meiosis stage (**[B]** and **[H]**), young microspore stage (**[C]** and **[I]**), vacuolated pollen stage (**[D]** and **[J]**), early pollen mitosis stage (**[E]** and **[K]**), and late pollen mitosis stage **(F)**. **(L)** shows a cross section of a *wda1* as-2 anther at the early pollen mitosis stage. BP, binucleated pollen; DMC, degenerated meiocyte; DMY, degenerated young microspore; En, endothecium cell layer; Ep, epidermis cell layer; M, middle layer; MC, meiocyte; SC, sporogenous cell; T, tapetal cell layer; TP, trinucleated pollen; UP, uninucleated pollen; YM, young microspore. Bars = 10 μm.

contracted (Figure 4H) and the number of small vesicles in the meiocytes increased (see Supplemental Figure 2 online). However, the overall structure and components of the anther wall was similar to that of the wild type (Figures 4B, 4H, 5A, and 5E).

At the end of meiosis, the wild-type meiocytes formed tetrads and free microspores were released into the anther locule. Tetrads or dyads also began to deposit exine on the intine (see Supplemental Figure 2 online), and orbicules (Ubisch bodies) started to appear in the peritapetal region (Figures 5B and 5J). In *wda1* anthers, tetrads did not develop normally (Figure 4I). Degenerated meiocytes formed thicker intines, but no exine deposition was observed in those mutants (see Supplemental Figure 2 online).

At the young microspore stage (Figure 4C), the microspores were developed and exine deposition continued in wild-type anthers. Sporopollenins were deposited to microspores to form the bacular and nexine of exine (see Supplemental Figure 2 online). The peritapetal region contained thick orbicules for the transfer of lipids and proteins from the tapetum. In addition,

Figure 3. (continued).

(A) Temporal and spatial expression patterns of the *Wda1-GUS* fusion product in heterozygous spikelets at various flowering stages. Sample 1, premeiosis; sample 2, meiosis; sample 3, tetrads; sample 4, young microspore; sample 5, vacuolated pollen; sample 6, early pollen mitosis; sample 7, late pollen mitosis.

(B) Photograph taken after removal of the palea and half of the lemma from the spikelet at the tetrad stage.

(C) Photograph taken after removal of the palea and half of the lemma from the spikelet at the vacuolated pollen stage.

(D) Anther at early pollen mitosis.

(E) Palea and lodicule at early pollen mitosis.

(F) Other side of the palea and lodicule in **(E)**.

(G) Magnified image of sample 7 in **(A)**.

(H) Cross section of a palea at the vacuolated pollen stage (sample 5 in **[A]**).

(I) Cross section of the lower portion of a spikelet at the vacuolated pollen stage (sample 5 in **[A]**).

(J) Cross section of an anther at the vacuolated pollen stage (sample 5 in **[A]**).

(K) Temporal expression patterns of *Wda1* in shoots and roots of 7-d-old seedlings, various stages of panicles, developing seeds at 6 d after pollination, and flag leaves.

(L) Spatial and temporal expression patterns of *Wda1* in developing wild-type anthers at five different stages (meiosis, young microspore, vacuolated pollen, pollen mitosis, and heading), palea/lemma, and lodicules/ovaries. *Ubq1* was used as a control. Data are representative of three independent experiments.

Photographs in **(H)** to **(J)** were taken under dark-field microscopy. A, anther; AF, anther filament; C, carpel; Co, cortex; CT, cortical tissue; En, endothecial cell layer; Ep, epidermal cell layer; FL, flag leaf; G, glumes; H, heading; IE, inner epidermis; Le, lemma; Lo, lodicule; M, meiosis; O, ovary; OE, outer epidermis; P, pollen; Pa, palea; PM, pollen mitosis; S, shoot of seedling at 7 d after germination; Se, developing seeds at 6 d after pollination; St, stigma; T, tapetal cell layer; Tr, trichome; V, vacuolated pollen; Va, vascular bundle; *wda1*, *wda1* homozyous anther; Y, young microspore. Bars = 1 mm in **(A)** to **(F)** and 20 μm in **(G)** to **(J)**.

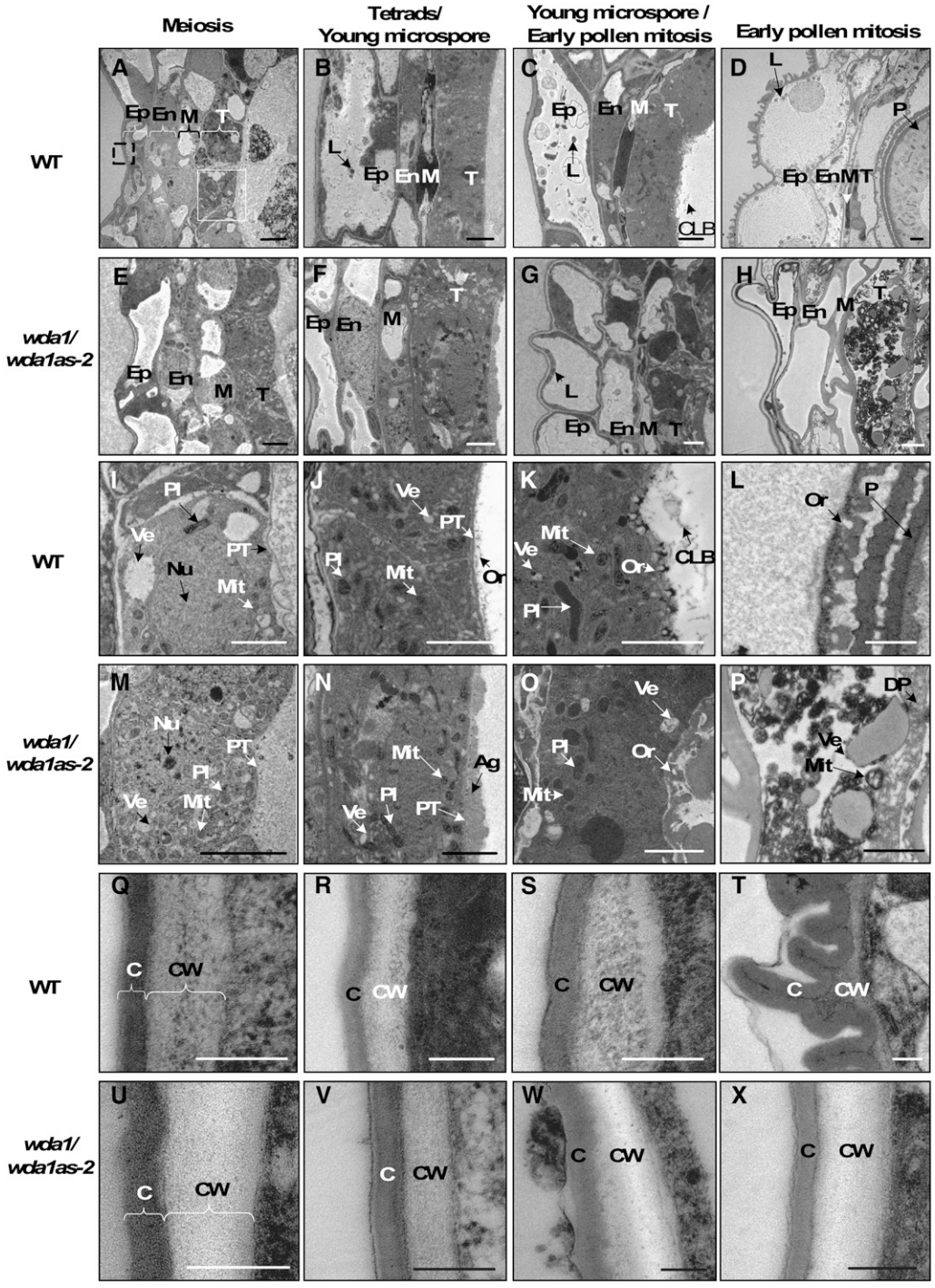

Figure 5. Transmission Electron Microscopy Analyses in Developing Anther Walls.

(A) to **(D)** Cross sections of wild-type anther walls at meiosis **(A)**, tetrad **(B)**, young microspore **(C)**, and early pollen mitosis **(D)** stages.
(E), **(F)**, and **(H)** Cross sections of *wda1* anther walls at meiosis **(E)**, young microspore **(F)**, and early pollen mitosis **(H)** stages.
(G) Cross section of a *wda1* as-2 anther wall at the early pollen mitosis stage.
(I) to **(L)** Magnified images of the peritapetal region in **(A)** to **(D)**.
(Q) to **(T)** Magnified images of the outer epidermal region in **(A)** to **(D)**.
(M) to **(P)** Magnified images of the peritapetal region in **(E)** to **(H)**.
(U) to **(X)** Magnified images of the outer epidermal region in **(E)** to **(H)**.
The white box in **(A)** indicates the peritapetal region, and the dotted black box indicates the outer epidermal region. Ag, aggregates; C, cuticle; CLB, cytoplasmic lipid body; CW, cell wall; DP, degenerated pollen; En, endothecium cell layer; Ep, epidermis cell layer; L, lipid body; M, middle layer; Mit, mitochondrion; Nu, nucleus; Or, orbicule; P, pollen; Pl, plastid; PM, plasma membrane; PT, peritapetal region; T, tapetal cell layer; Ve, vesicle; *wda1*, *wda1* homozygous anther; *wda1* as-2, *wda1* antisense-2 anther; WT, wild-type segregant. Bars = 5 μm in **(A)** to **(P)** and 0.2 μm **(Q)** to **(X)**.

cytoplasmic lipid bodies became visible (Figures 5C and 5K). However, the outer region of the anther epidermis was not much different from that in previous stages, except that a thin and darkly stained region developed in the outermost layer of the anther at the young microspore stage (Figures 5Q to 5S). By contrast, the *wda1* tapetum did not produce orbicules at the peritapetal region but showed some aggregated lipidic molecules (Figures 5F and 5N). Another characteristic of the mutant anthers was that their middle layers did not degenerate (Figures 5F and 5H). At the vacuolated pollen stage (Figure 4D), the microspores finished their exine deposition, started to deposit pollen coats into the tectum of exines, and began to enrich the pollen cytoplasm (see Supplemental Figure 2 online).

At the pollen mitosis stage in wild-type anthers (Figures 4E and 4F), the uninucleate pollen developed into trinucleate pollen through two mitotic divisions. Simultaneously, starches, proteins, lipids, and other nutrients enriched the pollen cytoplasm. Tapetal cells were completely degenerated by this stage, and maturation of the pollen wall finished. The endothecial cell layers finally disrupted to release mature pollen grains. Transmission electron microscopy analysis at the early pollen mitosis stage showed that the peritapetal region contained orbicules loaded with thick lipidic molecules (Figure 5L). The outermost epidermal layer had hair-like extensions from the cuticle layer, and numerous lipid bodies appeared in the epidermis (Figures 5C and 5D). However, we did not observe further development in the cuticle layer of the *wda1* epidermis (Figure 5X) because of a lack of lipid bodies with dark-stained lipidic molecules (Figure 5H). The *wda1* anthers were also severely shrunken at this stage, and most pollen grains degenerated in the anther locules (Figures 4J and 4K). In particular, the *wda1* tapetum accumulated irregularly shaped vesicles surrounded by dark-stained lipidic molecules; many degenerating mitochondria also aggregated around these vesicles (Figures 5H and 5P).

At the young microspore stage in wild-type tapeta, we observed regular patterns of lipidic molecules embedded in small vesicles, which were expected to be fused to the orbicules (Figure 5K). Moreover, we found no components of the degenerated tapeta at the pollen mitosis stage (Figures 5D and 5L). The *wda1* anthers had a similar phenotype after the vacuolated pollen stage. Mutant anthers did not dehisce because their tapeta were not degenerated (Figure 5H).

Close observation of anthers of the *wda1* antisense plants (as-2) at the early pollen mitosis stage showed an abnormally thick aggregation of sporopollenin in the pollen walls as well as undeveloped pollen cytoplasm (Figure 4L; see Supplemental Figure 2 online). Orbicules were generated similar to those in the wild type, although most were partially destroyed and, likely, incomplete (Figure 5O). In the epidermal layer of as-2, lipid bodies were abnormally incorporated in the cell wall and an abnormal cuticle layer was formed (Figures 5G and 5W). These antisense plants confirmed that the reduction in *Wda1* expression causes the abnormal development of anthers and microspores.

These observations suggest that phenotypic alterations in *wda1* probably result from blocked biosynthesis of lipidic molecules in the anther walls and, consequently, their hindered transference from the anther walls to the developing microspores and the cuticular layer of the anther.

wda1 Lacks Wax Crystals and Is Affected in Expansion and the Morphology of Anther Epidermal Cells

Our *wda1* knockout and antisense anthers were much shorter than those of the wild-type segregants (Figure 1B). However, this reduction in length is not a common phenomenon in male-sterile plants (Aarts et al., 1997; Ariizumi et al., 2004; Jung et al., 2005). Because *Wda1* is expressed strongly in the anther epidermis, we examined the surface structure of *wda1* anthers by scanning electron microscopy. Mutant anther walls appeared smooth compared with wild-type walls (Figures 6B, 6C, 6G, and 6H). Close examination of the wild-type anthers showed surfaces covered by epicuticular wax crystals, primarily linear and plate-shaped (Figure 6F). By contrast, the *wda1* knockout anthers contained no wax crystals (Figure 6G). The as-2 anthers had an intermediate level of plate-shaped epicuticular wax crystals (Figure 6H). In addition, the epidermal cells in *wda1* knockout and as-2 anthers were significantly shorter than those in the wild type (Figure 6F to 6H). However, the cell width of *wda1* was not much different from that of the wild type. These observations are also consistent with recent reports that mutations in the *Arabidopsis Long-Chain Acyl-CoA Synthetase* gene (At1g49430) and the *Arabidopsis ECR* gene (At3g55360), both involved in wax biosynthesis, affect the expansion of leaf epidermal cells (Schnurr et al., 2004; Zheng et al., 2005).

Although pollen development was severely hampered in the *wda1* anthers, pollen grains were rarely seen at the mature anther stage. Scanning electron microscopy analyses of those grains showed that they were much smaller than wild-type pollen and appeared to lack the exine (Figures 6D and 6E). The germination pores of the wild-type pollen were easily distinguished from other regions loaded with exine. In contrast, pores in the *wda1* pollen were not as easily identified because of the lack of exine on the walls (Figures 6D and 6E).

Major Components of Waxes Are Reduced in *wda1* Anthers

From the previous scanning electron microscopy analysis, we observed defective epicuticular waxes in *wda1* anthers. Using gas–liquid chromatography, we analyzed the composition and quantity of chloroform-extractable cuticular waxes in wild-type anthers (Table 1, Figure 7A). In contrast with leaf waxes, which were composed predominantly of long-chain alcohols and aldehydes (see Supplemental Figure 3 online), the major wax monomers in wild-type anthers were alkenes and alkanes (Table 1), with longer chains dominating in the former (C29, C31, and C33) compared with the latter (C25, C27, and C29) (Figure 7A; see Supplemental Table 1 online). These products of the decarbonylation pathway represented 87.29% of the total wax load, compared with 11.06% fatty acids and 1.65% alcohols as products of acyl reduction (Table 1).

For this analysis, we used whole anther samples, comprising both anther walls and pollen. However, as Figure 4 indicates, pollen development was affected in the *wda1* mutant. To determine whether these aliphatics or different aliphatics were also involved in forming the pollen surface, we analyzed the composition of waxes in the anther walls and pollen grains separately. Comparable high levels of alkanes and alkenes on the pollen and

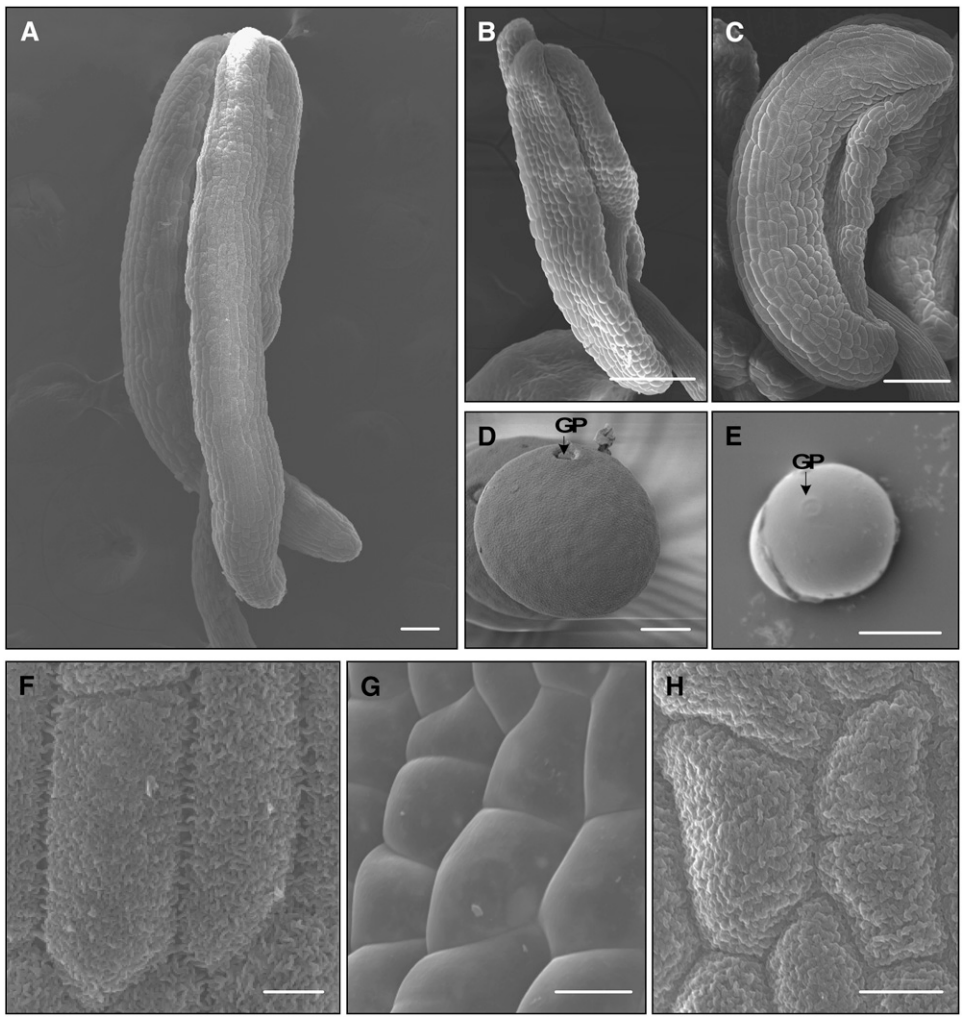

Figure 6. Scanning Electron Microscopy Analysis of Wild-Type and *wda1* Mutant Plants.

(A) Wild-type anther at the early pollen mitosis stage.
(B) *wda1* anther at the early pollen mitosis stage.
(C) *wda1* as-2 anther at the early pollen mitosis stage.
(D) Wild-type pollen at the early pollen mitosis age.
(E) *wda1* pollen at the early pollen mitosis stage.
(F) Outer epidermal region of a wild-type anther at the early pollen mitosis stage.
(G) Outer epidermal region of a *wda1* anther at the early pollen mitosis stage.
(H) Outer epidermal region of a *wda1* as-2 anther at the early pollen mitosis stage.
GP, germination pore. Bars = 100 μm in **(A)** to **(C)**, 5 μm in **(D)** and **(E)**, and 10 μm in **(F)** to **(H)**.

anther walls indicated that surface waxes in our rice anthers and pollen were very similar in their monomer composition, which are mostly very-long-chain alkenes and alkanes (see Supplemental Figure 4 online). The only differences are the lack of long-chain fatty acids and primary alcohols in the pollen, probably because carboxylated and hydroxylated aliphatics were polymerized into the highly resistant sporopollenin of the pollen wall. These results are consistent with those reported by Wilmesmeier and Wiermann (1995), in which very-long-chain alkanes and alkenes were the major compounds in maize pollen grains.

Consistent with the lack of wax crystals observed by scanning electron microscopy (Figure 6G), wax loads on *wda1* anthers were reduced to 23.34% of the wild-type level (Table 1). Similar levels of reduction in wax amounts have been observed in other mutants with waxless phenotypes (Jenks et al., 1995). Even so, the strongest effects of the *wda1* mutation on wax constituents were apparent in the unsaturated alkenes; the saturated alkanes, acids, and alcohols were also reduced (Table 1, Figure 7A). However, we were unable to observe any specific reduction in certain compound classes or for compounds of a certain chain length, indicating that the *Wda1* gene product is involved in the

Table 1. Wax Composition of Anthers from Wild-Type and *wda1* Mutant Plants

	Wild Type	*wda1*
Wax	[μg/mg (%)]	[μg/mg (%)]
Fatty acids	1.44 ± 0.06 (11.06)	0.28 ± 0.04 (9.58)
Alcohols	0.22 ± 0.03 (1.65)	0.08 ± 0.01 (2.90)
Alkanes	4.28 ± 0.15 (32.70)	1.61 ± 0.38 (52.30)
Alkenes	7.17 ± 0.79 (54.59)	1.09 ± 0.33 (35.21)
Total	13.11 ± 0.84 (100.00)	3.06 ± 0.65 (100.00)

Values shown are means ± SD ($n = 4$).

biosynthesis of all anther waxes. Consistent with the weak expression of *Wda1* in the vegetative organs, no significant qualitative or quantitative differences were seen in the leaf wax monomer composition of the wild-type and *wda1* seedlings (see Supplemental Figure 3 online).

Cutin Characteristic Monomers Are Reduced in *wda1* Anther Polyester

Consistent with *Wda1* expression in anther epidermal cells (Figure 3J), *wda1* anthers were defective in their epidermal cell wall formation, especially in the outermost portion of the cell wall (Figure 6G), which is typically characterized by the presence of a cuticle (i.e., the continuous layer of cutin secreted by the epidermis). Therefore, we wanted to investigate the role of *Wda1* in cuticle formation by analyzing the aliphatic monomer composition of *wda1* cutin compared with the wild type. However, traditional methods using polysaccharide hydrolases to isolate cuticles for subsequent depolymerization and analysis cannot be applied on the microscopic scale of anthers and pollen. Alternative approaches have now been demonstrated with the transesterification of polyester from delipidated tissue, resulting in a monomer composition representative of cutin (Bonaventure et al., 2004; Franke et al., 2005).

Analysis of the depolymerization products after transesterification revealed that rice anther polyester was composed predominantly of C16 and C18 oxygenated fatty acid derivatives. Of these, the most abundant compounds identified in the methanolysate were the cutin characteristic monomers 9(10), 16-dihydroxy-hexadecanoic acid, 18-hydroxy-octadecanoic acid, 9-epoxy-18-hydroxy-octadecanoic acid, and 16-hydroxy-hexadecanoic acid (Figure 7B; see Supplemental Figure 5 online). Minor compounds included 9(10),18-dihydroxy-octadecanoic acid, octadecene-1,18-dioic acid, hexadecane-1,16-dioic acid, octadecanoic acid, and eicosanoic acid. Another three compounds with gas chromatography (GC) retention times different from those of the identified monomers were released from the anthers by transesterification. These compounds had mass spectra compatible with hydroxylated fatty acids (see Supplemental Figure 5 online), indicating that they represent unknown rice cutin monomers (URCM1, URCM2, and URCM3). Because of the lack of available standards and very little understanding of the cutin monomer composition in grasses, the exact structures of these unknown rice cutin monomers remain to be determined.

The analysis of the aliphatic monomer composition of *wda1* anther methanolysates revealed that the *wda1* anther polyester is strongly reduced in cutin characteristic monomers. Compared with the wild type, all detected cutin monomers are decreased by at least 50%, indicating that *Wda1* is also involved in the pathways providing aliphatic precursors for proper cuticle formation.

In contrast with our analysis of whole anthers (Figure 7), comparison of the transesterification products of pollenless anther walls and isolated pollen (see Supplemental Figure 4 online) showed that almost no cutin monomers can be released from pollen by transesterification. This finding suggests that these functionalized aliphatics are incorporated into the highly resistant sporopollenin, which is required for proper exine formation.

Mutation in the *Wda1* Gene Affects the Expression of Rice *Raftin* Genes

To compare the functional roles of *Wda1* with those of other genes involved in pollen wall formation, we examined their expression levels in mutant anthers. Os *Raftin1* and Os *Raftin2* are highly similar to wheat *RAFTIN1*, a gene that plays important roles in exine maturation. RNA-induced gene-silenced lines of wheat *RAFTIN1* or Os *Raftin1* in rice showed male-sterile phenotypes attributable to arrested tapetal degeneration at the vacuolated pollen stage. Mutant anthers are nondehiscent and 10 to 15% shorter (Wang et al., 2003). These phenotypes are similar to those of *Wda1*. The gene product appears to function in transporting various molecules from the tapetum to pollen walls via orbicules (Wang et al., 2003). Our analyses showed that both rice *Raftin* genes were strongly expressed in the anthers (Figure 8). Whereas Os *Raftin1* was expressed throughout anther development, Os *Raftin2* was preferentially expressed at the early stages. In *wda1* anthers, Os *Raftin2* transcript was nearly undetectable, whereas that of Os *Raftin1* was reduced significantly. Therefore, the defect in wax production affected the expression of both rice *Raftin* genes and pollen fertility.

We also examined the expression of Os *Dex1*, which shares 70% identity with *Arabidopsis DEX1*, a gene essential for early pollen wall formation through exine patterning. Plants containing the *dex1* mutation exhibited alterations in their microspore membrane and primexine formation, thereby preventing normal deposition of sporopollenin and leading to male sterility (Paxson-Sowders et al., 2001). Quantitative RT-PCR analysis showed that the levels of Os *Dex1* transcript were unchanged in *wda1* anthers (Figure 8). We believe that WDA1 protein is involved in the biosynthesis of sporopollenin rather than the patterning of exine.

To find other components of the VLCFA biosynthesis genes in rice anthers, we analyzed lipid biosynthesis–related genes from previously reported microarray data (Kunst and Samuels, 2003; Jung et al., 2005) using the program for gene ontology (GO; http://www.geneontology.org/GO.slims.shtml) and clusters of orthologous groups of proteins (COG; http://www.ncbi.nlm.nih.gov/COG/). These analyses identified several anther-preferential genes that potentially encode acyl-CoA synthases, enoyl-CoA hydratase, ATP binding cassette (ABC) transporters, acyl carrier

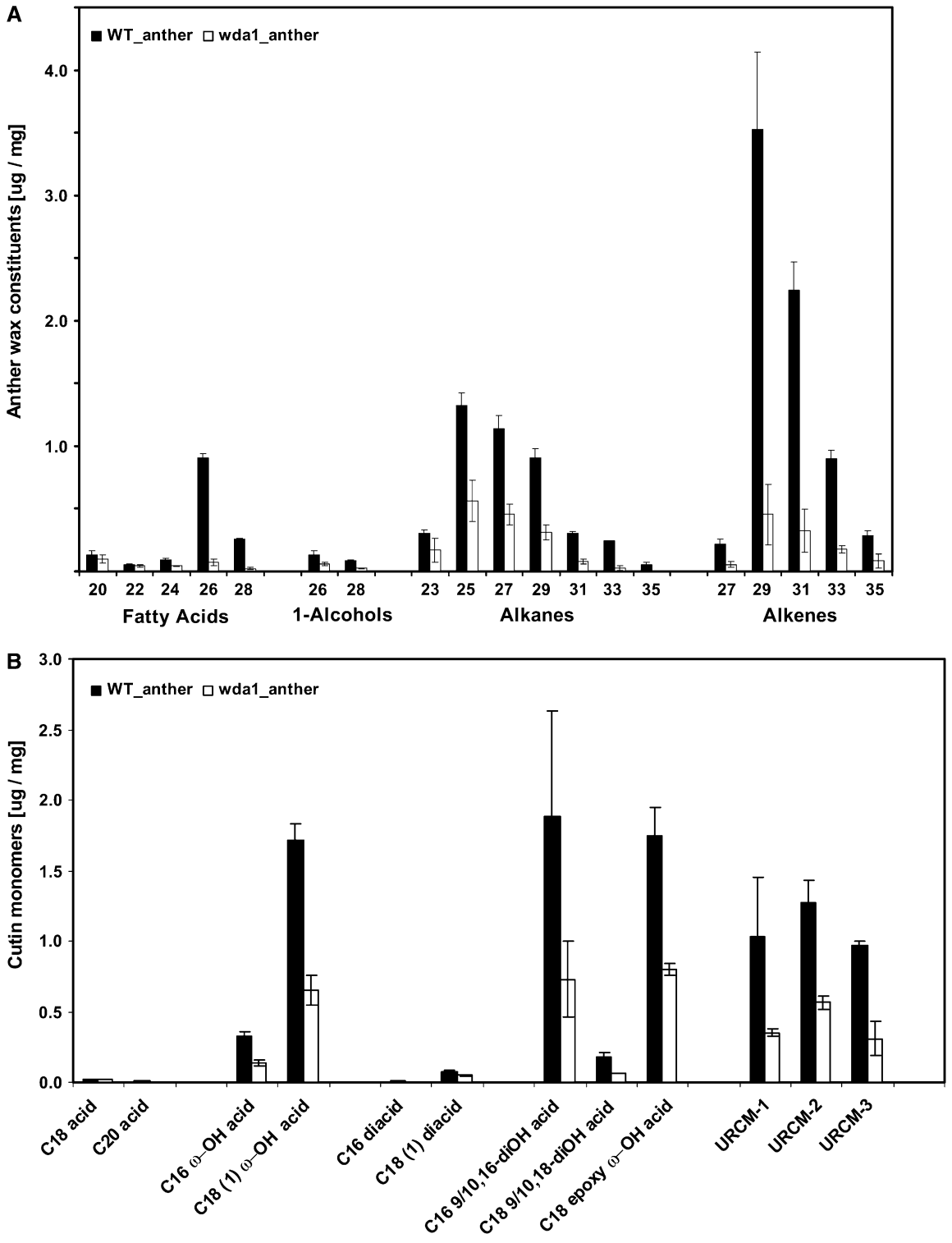

Figure 7. Wax and Cutin Constituents of Wild-Type and *wda1* Mutant Anthers.

(A) Wax analysis of wild-type and *wda1* whole anthers.

(B) Cutin analysis of wild-type and *wda1* whole anthers.

White bars represent levels of each compound in the *wda1* mutant, and black bars represent them in the wild type. Error bars indicate SD ($n = 4$). Compound names are abbreviated as follows: C18 acid, octadecanoic acid; C20 acid, eicosanoic acid; C16 ω-OH acid, 16-hydroxy-hexadecanoic acid; C18 (1) ω-OH acid, 18-hydroxy-octadecanoic acid; C16 diacid, hexadecane-1,16-dioic acid; C18 (1) diacid, octadecene-1,18-dioic acid; C16 9/10,16-diOH acid, 9(10),16-dihydroxy-hexadecanoic acid; C18 9/10,18-diOH acid, 9(10),18-dihydroxy-octadecanoic acid; C18 epoxy ω-OH acid, 9-epoxy-18-hydroxy-octadecanoic acid; URCM, unknown rice cutin monomer. Acids were analyzed as methyl esters, and hydroxyl groups were analyzed as trimethylsilyl esters.

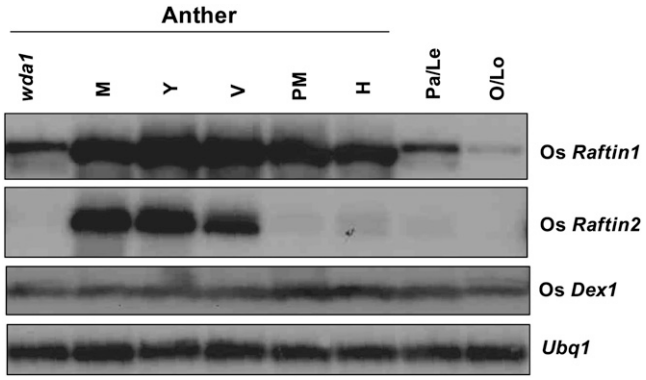

Figure 8. Effect of the *wda1* Mutation on Exine-Related Genes.

Semiquantitative RT-PCR analyses of exine-related genes (Os *Raftin1*, Os *Raftin2*, and Os *Dex1*). RNA samples were prepared from *wda1* anthers and from various stage anthers, palea/lemma, and lodicules/ovaries from wild-type spikelets. *Ubq1* served as a control. Bands shown are RT-PCR products. The experiment was repeated at least three times, and data from one representative experiment are shown. H, heading; Le, lemma; Lo, lodicule; M, meiosis; O, ovary; Pa, palea; PM, pollen mitosis; Y, young microspore; V, vacuolated pollen.

proteins, fatty acyl-CoA elongase, and acyl-CoA reductases, all of which might be involved in wax biosynthesis (see Supplemental Table 2 online) (Aarts et al., 1997; Hooker et al., 2002; Kunst and Samuels, 2003; Pighin et al., 2004; Zheng et al., 2005). Among these, expression of an acyl-CoA synthase gene and an acyl-CoA reductase gene was downregulated in *wda1* anthers (see Supplemental Figure 6 online). Interestingly, the 3-ketoacyl-CoA synthase gene, which is expected to have a major role in the VLCFA biosynthesis pathway, showed strong expression in anthers. By contrast, fatty acyl-CoA reductase genes that are involved in the acyl reduction pathway, a minor portion of VLCFA biosynthesis in anthers, showed weak expression even though the expression level was examined after 35 cycles via semiquantitative RT-PCR (see Supplemental Figure 6 and Supplemental Table 2 online) (Aarts et al., 1997).

DISCUSSION

In this study, we identified a T-DNA insertion mutant in *Wda1*, a rice homolog of *Arabidopsis CER1*. *CER1* and homologous genes, such as *WAX2* and *GL1*, are involved in cuticle formation or wax deposition (Jenks et al., 1995; Hansen et al., 1997; Chen et al., 2003). Although conditional male sterility was observed in stem wax–deficient *Arabidopsis* mutants, the functional studies related to CER1 and homologous genes were focused on biochemical or developmental roles in leaves or stems (Aarts et al., 1995; Fiebig et al., 2000). Interestingly, the *wda1* mutant exhibits developmental and biochemical phenotypes that reveal the functioning of *Wda1* in the epidermal layer and tapetum of the anther wall, the orbicule in the peritapetal region and pollen development, and the biosynthesis of VLCFA derivatives required for cuticle formation and wax deposition.

Wda1 Is Preferentially Expressed in Epidermis of Various Floral Organs, including Anthers

The *Wda1* gene was identified as a *Wda1-GUS* fusion in the line that showed strong GUS expression in various floral organs, especially the anther walls, trichomes, inner and outer epidermis of the palea/lemma, and surfaces of stigmas and lodicules (Figure 3). The GUS expression patterns suggest that *Wda1* functions in the outer cell layers of the floral organs (Figures 3H and 3J). However, its reduced expression causes phenotypic alterations only in the anthers and not in other floral organs in which it is expressed. In those organs, such as the palea/lemma, other genes might compensate for mutations in the *Wda1* gene. Two genes—LOC_Os02g40780 and LOC_Os02g56920—that are highly similar to *Wda1* are present in the rice genome. Compared with *Wda1*, both are expressed only weakly in flowers but strongly in the vegetative tissues (Figures 3K and 3L; see Supplemental Table 3 online). Their expression may be sufficient to compensate for the *wda1* defects in most vegetative and most floral organs. In vegetative organs, *Wda1* is only weakly expressed and can be detected only in collar regions and basal parts around the shoot apical meristem (see Supplemental Figure 1 online). Perhaps *wda1* defects in these areas may not be fully compensated for by other genes, thereby exhibiting the smaller and less tiller phenotypes (Figure 1A). Even though there were slight defects of growth in *wda1* plants, *Wda1* is primarily required for the developmental processes involved in anther and pollen maturation. Publicly available expression data (UniGene Cluster: http://www.ncbi.nlm.nih.gov/UniGene/UGOrg.cgi?TAXID=4530) indicate that *Wda1* ESTs were predominant in the panicles but that ESTs of LOC_Os02g40780 were present in various organs (e.g., callus, leaf/stem, and flower) (see Supplemental Table 3 online). ESTs of another *Wda1*-related gene, LOC_Os02g56920, were abundant in both vegetative organs and flowers. This UniGene Cluster information supports the notion that *Wda1* expression is panicle-preferential, whereas its related genes are more widely expressed in both vegetative and reproductive stages.

WDA1 Functions in the Biosynthesis of Various VLCFA Precursors for Wax and Cutin Monomers

The importance of VLCFA biosynthesis in plants for fertility and development in reproductive organs, such as anthers and pollen, has been reported for wax-deficient mutants or mutants in lipid biosynthesis in the dicotyledonous Brassicaceae, including *Arabidopsis* (Aarts et al., 1997; Hernandez-Pinzon et al., 1999; Fiebig et al., 2000; Ariizumi et al., 2003, 2004). However, related studies are rare in monocotyledonous plants (Wang et al., 2002). Based on the phylogenic analysis (Figure 2C), a biochemical function similar to that of *Arabidopsis* CER1, proposed to be involved in the decarbonylation pathway of stem wax biosynthesis (Aarts et al., 1995), could be expected for WDA1. However, WAX2 and GL1, other proteins similar to WDA1, are suggested to be involved in transporting various lipidic molecules or acting as a membrane-bound receptor, respectively (Jenks et al., 1995; Hansen et al., 1997; Chen et al., 2003; Kunst and Samuels, 2003), leaving the biochemical function of CER1-like proteins still unclear.

Analysis of the chloroform-extractable cuticular waxes of rice wild-type anthers and pollen grains showed that the major wax components in anthers and pollen are very-long-chain alkenes and alkanes (Figure 7A; see Supplemental Figure 4 online), similar to those found for maize pollen (Wilmesmeier and Wiermann, 1995). In *wda1* anthers, these lipid levels are reduced to 23.34% (Table 1). These lipid defects and the observation of GUS activity in the anther wall indicate that WDA1 should have a significant role in the generation or secretion of very-long-chain aliphatic molecules, including the precursors for sporopollenin in anther walls. Because of the very pronounced reduction of unsaturated alkenes in *wda1*, it is tempting to speculate that WDA1 acts as a desaturase in the pathways to very-long-chain aliphatics, consistent with the three N-terminal His-rich motifs conserved in WDA1 and other desaturases (Taton et al., 2000). However, because saturated alkanes are also reduced significantly in *wda1*, a less specific function of WDA1 is more likely. In addition, a catalytic function of WDA1 specific for intermediates of the decarbonylation pathway, as proposed for CER1 (Aarts et al., 1995), is unlikely, because very-long-chain (C26 and C28) fatty acids and alcohols, products of the acyl reduction pathway, are also reduced significantly in *wda1* anthers (Figure 7A). Therefore, WDA1 is potentially involved in the general processes of VLCFA biosynthesis. The latter hypothesis is supported by the fact that the amount of all cutin monomers is reduced severely in the methanolysate of *wda1* anther polyester (Figure 7B). The decrease in monomers of various substance classes and monomers of different chain lengths strongly indicates that WDA1 participates in the modification of more than one aliphatic precursor. This is consistent with the broad range of activity observed in lipid metabolic enzymes, such as lipid desaturases, which have been shown to also function as hydroxylases (Broadwater et al., 2002). In addition, subcellular localization analysis using green fluorescent protein showed that WDA1 is targeted to the endoplasmic reticulum (see Supplemental Figure 7 online), similar to ECR, CER6, and GL8, which are part of the VLCFA elongase complex (Xu et al., 2002; Kunst and Samuels, 2003; Zheng et al., 2005). The desaturase motif in WDA1 would be consistent with a function for WDA1 as a dehydratase in an anther-specific fatty acid elongation complex for general lipid metabolism.

WDA1 Is Involved in the Regulation of Genes Related to Lipid Biosynthesis and Pollen Wall Development

Figures 5 and 6 demonstrate that WDA1 is involved in pollen and anther development, possibly via effects on the synthesis or diffusion of signals, such as the lipidic signaling molecules (Aharoni et al., 2004) that direct pollen and anther development. This is indicated by the fact that genes potentially involved in lipid metabolism and transfer are downregulated in *wda1* anthers. Of them, we identified LOC_Os03g26600, a putative component of the rice fatty acid elongase complex, encoding KCS, which shows strong expression in rice anthers (Kunst and Samuels, 2003; Jung et al., 2005) (see Supplemental Table 2 online). It is significantly downregulated in the *wda1* anther (see Supplemental Figure 6 online). This KCS has 61% similarity to *Arabidopsis* KCS1, which is involved in wax biosynthesis (Todd et al., 1999). Downregulation of KCS in *wda1* anthers may also contribute to the overall differences in wax components between wild-type and mutant anthers. We also found that the Os *MS2* gene, with 73% similarity to At *MS2*, a key component of the acyl reduction pathway in *Arabidopsis* (Aarts et al., 1997), is preferentially expressed in the anther and is severely reduced in the *wda1* anther (see Supplemental Figure 6 online). Also indicative for *Wda1* functioning at the molecular level are effects on rice *Raftin* genes that are homologs of the wheat *RAFTIN1* gene located at orbicules and exines, which are supposed to have a guiding role in the proper fixation of sporopollenin polymers in the exine (Wang et al., 2003). Os *Raftin2* is preferentially expressed during early pollen development, whereas Os *Raftin1* functions at all stages in the wild-type anthers (Figure 8). The severe downregulation of both putative rice orbicule marker genes and the absence of orbicules and cytoplasmic lipid bodies in *wda1* anthers imply that the *wda1* mutant possibly affects the transfer of sporopollenin from the tapetum to the pollen walls via these organelles. Whether its effect on the expression of other lipid-related genes is direct (e.g., synthesis of signaling molecules) or indirect (e.g., downregulation of lipid-related genes by a feedback mechanism attributable to the accumulation of lipid precursors) can be clarified only by evaluating the biochemical function of WDA1. To date, all of our attempts have failed to heterologously express a functional WDA1 protein and determine catalytic activity.

WDA1 Is Required for Cell Expansion and Early Anther Development

Unlike most *cer* mutants or other VLCFA metabolism–related mutants with reduced fertility (Aarts et al., 1995; Fiebig et al., 2000; Pighin et al., 2004; Zheng et al., 2005), the major phenotypes for our *wda1* mutant were observed in the rice anther wall, epidermis, and tapetum and included severe morphological abnormalities and smaller anthers. As a result, *wda1* exhibited complete male sterility (Figure 1). A detailed examination of epidermal cells in the developing anther walls demonstrated that *wda1* and *wda1* as-2 cells are approximately four and two times smaller than wild-type cells, respectively, which is closely correlated with a similar reduction in anther size (Figure 6). In particular, expansion of the anther epidermal cell after the meiosis of male gametes did not proceed in *wda1* anthers. This early developmental defect was the likely cause of reduced organ sizes, similar to what has been reported for leaves from *Arabidopsis cer10* mutants (Zheng et al., 2005). It seems that this defect resulted from the blocked transport of VLCFA aliphatic moieties from the epidermal cell to the epicuticular wax layer via the lipid bodies (Figures 5H and 5X). Recently, CER5 was reported to encode an ABC transporter. It is thought to be involved in the transfer of cuticle wax constituents from epidermal cell walls to epicuticular or intracuticular wax layers. This kind of transporter is possibly involved in the formation of an epicuticular wax layer in the anther wall (Pighin et al., 2004), such as a rice putative CER5-like protein (e.g., LOC_Os10g35180, an ABC transporter) that is strongly expressed in anther through previous rice 60k oligomicroarray experiments (http://www.ggbio.com/) (see Supplemental Table 2 online). However, molecular and cellular mechanisms that regulate plant cell expansion during development still remain poorly understood, despite recent results from Zheng et al. (2005).

Developmental Roles for *Wda1* in the Rice Anther Wall

Before meiosis, the development of meiocytes and the four layers of the anther walls are nearly normal in *wda1* anthers. Plastid accumulation is also normal within the tapetum. During the young microspore stage in wild-type anthers, orbicules surrounded by thick lipidic molecules are easily distinguished at the peritapetal layer, and cytoplasmic lipid bodies occur in the locule. Exine of the pollen walls is formed by the deposition of molecules that are transferred from the developing tapetum via these orbicules and cytoplasmic lipid bodies (Piffanelli et al., 1998; Wang et al., 2003). By contrast, the tapetal layers of *wda1* mutants do not contain any orbicules or cytoplasmic lipid bodies, causing exine formation to fail.

The outer epidermal layer begins to accumulate epicuticular waxes after the vacuolated pollen stage. Generally, the cuticle consists of these epicuticular waxes and cutins in the epidermal layer. It is important for overcoming various environmental stresses, especially uncontrolled water loss. The *wda1* anthers, with defects in both components, are severely shrunken by dehydration and are easily damaged by physical forces (data not shown). This suggests that *Wda1* has a major role in enhancing the physical protection of anthers by generating epicuticular waxes and cutins. In addition, there is a difference between the growth patterns of wild-type and *wda1* anthers, and consequently, there is a difference in overall lipid content, resulting in a severe phenotype. To test this hypothesis, we examined the wax contents of another pollen-defect mutant (Os *Dex1* knockout) that shows an exine-defect phenotype similar to *Arabidopsis dex1*. Unlike *wda1*, Os *dex1* anthers did not display significant changes in surface lipid content (data not shown). Also, sequence analysis clearly shows that WDA1 is a lipid metabolic enzyme. However, we cannot exclude other possibilities that lipid content is reduced by the mutation.

This study reports on a mutant defective in the formation of cuticular waxes and cutins of anther walls. Therefore, this material will be valuable for studying the role of waxes in anther development and in response to various types of environmental stress.

METHODS

Plant Growth

Seeds of wild-type rice (*Oryza sativa* cv Japonica) and *wda1* were germinated on MSO medium containing 0.44% Murashige and Skoog basal salts, 3% sucrose, 0.2% Phytagel, and 0.55 mM *myo*-inositol (Sigma-Aldrich). The seedlings were grown for 1 week at 28°C under continuous light, then transplanted to soil in the greenhouse and raised to maturity.

Phylogenetic Analysis

Sequences similar to that of WDA1 were searched through BLAST in the GenBank protein database (http://www.ncbi.nlm.nih.gov/BLAST/), and the results were inspected manually. Sequences were aligned with ClustalW version 1.81, followed by manual alignment. Trees were constructed on conserved positions of the alignment by clustered protein sequences from plants with the neighbor-joining algorithm as implemented in MEGA 2.1 (Kumar et al., 2001) with pairwise deletion for gap filling. To test inferred phylogeny, we used bootstraps with 1000 bootstrap replicates. The tree was represented in the traditional rectangular form.

Histochemical GUS Assays and Microscopic Analyses

Histochemical GUS staining was performed as described by Jefferson et al. (1987) and Dai et al. (1996), except for the addition of 20% methanol to the staining solution. For light microscopic analysis, the tissues were fixed in a solution containing 50% ethanol, 5% acetic acid, and 3.7% formaldehyde, then embedded in Paraplast (Sigma-Aldrich) and Technovit 8100 resin (Heraeus). The samples were sectioned to 3- to 16-μm thickness with a microtome (Leica) and observed with a microscope (Nikon) using bright- and dark-field illumination.

Transmission Electron Microscopic Analysis

Spikelets and anthers of wild-type, *wda1*, and *wda1* as-2 mutant plants were sampled at various stages of development and fixed for 4 h in cacodylate buffer, pH 7.2, that contained 2% paraformaldehyde (Sigma-Aldrich) and 2% glutaraldehyde (Sigma-Aldrich). They were then rinsed with the same buffer and postfixed for 1 h in cacodylate buffer containing 1% osmium tetroxide (Pelco International). After dehydration, the specimens were embedded in London Resin White (London Resin). Ultrathin sections (40 to 60 nm thick) collected on uncoated nickel grids (300 mesh) were stained with 4% uranyl acetate and examined at 60 to 80 kV with a JEOL 1200 transmission electron microscope (JEOL).

Scanning Electron Microscopic Analyses

Spikelets of wild-type, *wda1*, and *wda1* as-2 plants were harvested, embedded for 4 h at 4°C in 0.1 M sodium phosphate buffer solution containing 3% glutaraldehyde, pH 6.8, rinsed three times in 0.1 M phosphate buffer, pH 6.8, and further fixed in 0.1 M sodium phosphate buffer solution containing 2% osmium tetroxide at 4°C overnight. They were rinsed again in the same buffer, dehydrated with an acetone series from 30 to 100% and then three times with 100% acetone, exchanged three times with isoamyl acetate (Sigma-Aldrich), processed for critical point drying using liquid CO_2, and gold-coated (10-nm thickness) in a SCD040 sputter coater (Balzers Union). The specimens were then examined in a LEO1450vp (Zeiss) with an accelerating voltage of 15 kV.

Semiquantitative RT-PCR and DNA Gel Blot Analyses

Total RNAs were isolated using Tri reagent (Molecular Research Center). The mRNAs were acquired with a PolyATtract mRNA isolation system (Promega). For first-strand cDNA synthesis, 200 ng of mRNA was reverse-transcribed in a total volume of 100 μL that contained 10 ng of oligo$(dT)_{12-18}$ primer, 2.5 mM deoxynucleotide triphosphate, and 200 units of Moloney murine leukemia virus reverse transcriptase (Promega) in a reaction buffer. PCR was performed in a 50-μL solution containing a 1-μL aliquot of the cDNA reaction, 0.2 μM of gene-specific primers, 10 mM deoxynucleotide triphosphates, 1 unit of ExTaq DNA polymerase (Takara), and reaction buffer. The reaction included an initial 5-min denaturation at 94°C, followed by 21 to 35 cycles of PCR (94°C for 45 min, 60°C for 45 min, and 72°C for 1 min), and a final 10 min at 72°C. Afterward, 20 μL of the reaction mixture was separated on a 1.2% agarose gel, blotted onto a nylon membrane, and hybridized with ^{32}P-labeled gene-specific probes. The specificity of the RT-PCR primers was verified by sequencing the PCR products. The primers used for RT-PCR are described in Supplemental Table 4 online.

Generating *Wda1* Antisense Plants

To generate *Wda1* underexpressed lines (*wda1* as-1 to as-5), the 653-bp N-terminal region of the *Wda1* cDNA was amplified by p1 (5′-ACAAACCCAGGACTCTTCACG-3′) and p2 (5′-GTAATGTTTGGAGCCTCGAGG-3′) primers (Figure 2A), and the PCR product was placed under the maize (*Zea mays*) ubiquitin promoter in the antisense direction. The construct was then placed in a binary Ti plasmid vector and introduced to rice calli via *Agrobacterium tumefaciens*–mediated transformation (Hiei et al., 1997; Lee et al., 1999).

Analysis of Anther and Leaf Waxes

Waxes were analyzed basically as described previously (Hauke and Schreiber, 1998). Two to 4 mg of freeze-dried anthers was submersed in 700 μL of chloroform for 1 min. The resulting chloroform extract was spiked with 10 μg of tetracosane (Fluka) as an internal standard and then transferred to a new vial. Any remaining insoluble anther material was used for our polyester analysis (see below). The solvent was evaporated under a nitrogen stream, and compounds containing free hydroxyl and carboxyl groups were converted to their trimethylsilyl ethers and esters with 20 μL of bis-(*N*,*N*-trimethylsilyl)-tri-fluoroacetamide (Machery-Nagel) in 20 μL of pyridine for 40 min at 70°C before gas chromatography–mass spectrometry (GC-MS) analysis. Monomers were identified from their electron ionization–mass spectrometry spectra (70 eV, *m/z* 50 to 700) after capillary GC (30-m × 0.32-mm × 0.1-μm film thickness [DB-1; J&W Scientific]; on-column injection at 50°C, oven temperature of 2 min at 50°C, increasing at 40°C/min to 200°C, 2 min at 200°C, increasing at 3°C/min to 310°C, 30 min at 310°C, and helium carrier gas at 2 mL/min) on an Agilent 6890N gas chromatograph combined with a 5973N quadrupole mass selective detector (Agilent Technologies). Quantitative determination of the wax components was performed with an identical GC system equipped with a flame ionization detector.

For the wax analysis of leaf tissues, several extraction conditions were applied based on previously described extraction methods (Bianchi et al., 1979; Welker and Haas, 1998). Here, the leaves were extracted under increasing temperature because Haas et al. (2001) reported that the polymeric aldehydes in rice leaf wax crystalloids become extractable only in heated chloroform (Haas et al., 2001). Briefly, 10-cm leaf blades were carefully dipped in 30 mL of chloroform for 10 s at room temperature and spiked with the internal standard tetracosane before a 3-mL aliquot of the chloroform extract was concentrated and derivatized as described above. In this extract, the major wax components, alcohols and esters, were detected, but aldehydes were present only in trace amounts. Therefore, the samples were immediately reextracted at 35°C, resulting in the detection of significant amounts of very-long-chain aldehydes and additional quantities of compounds detected in the previous extraction step. In an attempt to obtain insight into leaf polyester composition (not part of this study; data not shown), we further treated the leaf material as described below and included a depolymerization step at 80°C. Those hot extraction conditions resulted in substantial amounts of aldehydes being solubilized. Nevertheless, at each extraction step, no significant differences in the levels of any wax components were found between the wild-type and *wda1* samples. Therefore, we combined the data from all three extractions to represent the leaf wax composition.

Analysis of Cutin-Like Polyester in Rice Anthers

Analysis of the monomer composition of the anther polyester was performed as described by Franke et al. (2005). To ensure complete extraction of all soluble lipids, anthers that had been used in the wax extraction were reextracted in freshly added 700 μL of chloroform. They were first incubated at 50°C for 30 min, then overnight with constant shaking at room temperature. This extraction was repeated before the anthers were finally dried over silica. The delipidated anthers were then depolymerized using transesterification in 1 mL of 1 N methanolic HCl (Supelco) for 2 h at 80°C. This step released solvent-extractable methyl esters suitable for GC and GC-MS analysis. After the addition of 2 mL of saturated $NaCl/H_2O$, the hydrophobic monomers were subsequently extracted three times in hexane that contained 20 μg of internal standard (Dotriacontane; Sigma-Aldrich). The organic phases were then combined, evaporated, and derivatized as described above. GC-MS and GG–flame ionization detection analyses were performed as for the wax analysis, using a modified GC temperature program: on-column injection at 50°C, oven temperature of 2 min at 50°C, increasing at 10°C/min to 150°C, 1 min at 150°C, increasing at 3°C/min to 310°C, and 30 min at 310°C.

Accession Numbers

Sequence data for the genomic DNA and mRNA of *Wda1* have been deposited to the GenBank data library under accession numbers NT_080067 and NM_196959 (OSJNBa0079L16.17).

Supplemental Data

The following materials are available in the online version of this article.

Supplemental Figure 1. GUS Assay in Vegetative Organs and Developing Seeds.

Supplemental Figure 2. Transmission Electron Microscopy Analyses in Developing Pollen.

Supplemental Figure 3. Leaf Wax Constituents of Wild-Type and *wda1* Mutant Plants.

Supplemental Figure 4. Wax and Cutin Constituents of Rice Pollen and Anther Walls.

Supplemental Figure 5. GC-MS Analysis of Monomers Released from Cutin-Like Polyester in Rice Anthers by Methanolic HCl–Catalyzed Transesterification.

Supplemental Figure 6. Effect of the *wda1* Mutation on Possible Wax Biosynthesis–Related Genes.

Supplemental Figure 7. Subcellular Localization of WDA1.

Supplemental Table 1. Detailed Wax Constituents in the Anther, Anther Wall, and Pollen of Wild-Type and *wda1* Anthers.

Supplemental Table 2. Microarray Data Related to Wax Biosynthesis from a Previous Comparison between the Palea/Lemma and Developing Anthers.

Supplemental Table 3. Expression Patterns of Three Rice Genes in the Same Clade with CER1, Based on the Number of EST Clones in GenBank.

Supplemental Table 4. Primers Used for Semiquantitative RT-PCR Analyses.

Supplemental Table 5. Multiple Alignments of Plant Proteins Showing High Similarity with WDA1 Protein, as Presented in the Phylogenic Tree in Figure 2C.

ACKNOWLEDGMENTS

We thank In-Soon Park for generating the transgenic plants, Rod J. Scott (University of Bath), Pamela Ronald (University of California, Davis, CA), and Jong-Seong Jeon (Kyung Hee University) for helpful discussions, Sujin Kim for transmission electron microscopy analysis, and Priscilla Licht for English editing. This work was supported, in part, by grants

from the Crop Functional Genomic Center, the 21st Century Frontier Program (CG1111), and the Biogreen 21 Program, Rural Development Administration.

Received February 20, 2006; revised September 8, 2006; accepted October 30, 2006; published November 30, 2006.

REFERENCES

Aarts, M.G., Hodge, R., Kalantidis, K., Florack, D., Wilson, Z.A., Mulligan, B.J., Stiekema, W.J., Scott, R., and Pereira, A. (1997). The *Arabidopsis* MALE STERILITY 2 protein shares similarity with reductases in elongation/condensation complexes. Plant J. **12,** 615–623.

Aarts, M.G., Keijzer, C.J., Stiekema, W.J., and Pereira, A. (1995). Molecular characterization of the *CER1* gene of *Arabidopsis* involved in epicuticular wax biosynthesis and pollen fertility. Plant Cell **7,** 2115–2127.

Aharoni, A., Dixit, S., Jetter, R., Thoenes, E., van Arkel, G., and Pereira, A. (2004). The SHINE clade of AP2 domain transcription factors activates wax biosynthesis, alters cuticle properties, and confers drought tolerance when overexpressed in *Arabidopsis*. Plant Cell **16,** 2463–2480.

Ahlers, H., Thom, I., Lambert, J., Kuckuk, R., and Wiermann, R. (1999). ^{1}H NMR analysis of sporopollenin from *Typha angustifolia*. Phytochemistry **50,** 1095–1098.

Ariizumi, T., Hatakeyama, K., Hinata, K., Inatsugi, R., Nishida, I., Sato, S., Kato, T., Tabata, S., and Toriyama, K. (2004). Disruption of the novel plant protein NEF1 affects lipid accumulation in the plastids of the tapetum and exine formation of pollen, resulting in male sterility in *Arabidopsis thaliana*. Plant J. **39,** 170–181.

Ariizumi, T., Hatakeyama, K., Hinata, K., Sato, S., Kato, T., Tabata, S., and Toriyama, K. (2003). A novel male-sterile mutant of *Arabidopsis thaliana*, *faceless pollen-1*, produces pollen with a smooth surface and an acetolysis-sensitive exine. Plant Mol. Biol. **53,** 107–116.

Bianchi, G., Lupotto, E., and Russok, S. (1979). Composition of epicuticular wax of rice, *Oryza sativa*. Experientia **35,** 1417.

Bonaventure, G., Beisson, F., Ohlrogge, J., and Pollard, M. (2004). Analysis of the aliphatic monomer composition of polyesters associated with *Arabidopsis* epidermis: Occurrence of octadeca-cis-6,cis-9-diene-1,18-dioate as the major component. Plant J. **40,** 920–930.

Broadwater, J.A., Whittle, E., and Shanklin, J. (2002). Desaturation and hydroxylation. Residues 148 and 324 of *Arabidopsis* FAD2, in addition to substrate chain length, exert a major influence in partitioning of catalytic specificity. J. Biol. Chem. **277,** 15613–15620.

Chen, X., Goodwin, S.M., Boroff, V.L., Liu, X., and Jenks, M.A. (2003). Cloning and characterization of the *WAX2* gene of *Arabidopsis* involved in cuticle membrane and wax production. Plant Cell **15,** 1170–1185.

Dai, Z., Gao, J., An, K., Lee, J.M., Edwards, G.E., and An, G. (1996). Promoter elements controlling developmental and environmental regulation of a tobacco ribosomal protein gene *L34*. Plant Mol. Biol. **32,** 1055–1065.

Dietrich, C.R., Perera, M.A., D Yandeau-Nelson, M., Meeley, R.B., Nikolau, B.J., and Schnable, P.S. (2005). Characterization of two GL8 paralogs reveals that the 3-ketoacyl reductase component of fatty acid elongase is essential for maize (*Zea mays* L.) development. Plant J. **42,** 844–861.

Fiebig, A., Mayfield, J.A., Miley, N.L., Chau, S., Fischer, R.L., and Preuss, D. (2000). Alterations in *CER6*, a gene identical to *CUT1*, differentially affect long-chain lipid content on the surface of pollen and stems. Plant Cell **12,** 2001–2008.

Franke, R., Briesen, I., Wojciechowski, T., Faust, A., Yephremov, A., Nawrath, C., and Schreiber, L. (2005). Apoplastic polyesters in *Arabidopsis* surface tissues—A typical suberin and a particular cutin. Phytochemistry **66,** 2643–2658.

Guilford, W.J., Schneider, D.M., Labovitz, J., and Opella, S.J. (1988). High resolution solid state ^{13}C NMR spectroscopy of sporopollenins from different plant taxa. Plant Physiol. **86,** 134–136.

Haas, K., Brune, T., and Rücker, E. (2001). Epicuticular wax crystalloids in rice and sugar cane leaves are reinforced by polymeric aldehydes. J. Appl. Bot. **75,** 178–187.

Hansen, J.D., Pyee, J., Xia, Y., Wen, T.J., Robertson, D.S., Kolattukudy, P.E., Nikolau, B.J., and Schnable, P.S. (1997). The glossy1 locus of maize and an epidermis-specific cDNA from *Kleinia odora* define a class of receptor-like proteins required for the normal accumulation of cuticular waxes. Plant Physiol. **113,** 1091–1100.

Hauke, V., and Schreiber, L. (1998). Ontogenetic and seasonal development of wax composition and cuticular transpiration of ivy (*Hedera helix* L.) sun and shade leaves. Planta **207,** 67–75.

Hernandez-Pinzon, I., Ross, J.H., Barnes, K.A., Damant, A.P., and Murphy, D.J. (1999). Composition and role of tapetal lipid bodies in the biogenesis of the pollen coat of *Brassica napus*. Planta **208,** 588–598.

Hiei, Y., Komari, T., and Kubo, T. (1997). Transformation of rice mediated by *Agrobacterium tumefaciens*. Plant Mol. Biol. **35,** 205–218.

Hooker, T.S., Millar, A.A., and Kunst, L. (2002). Significance of the expression of the CER6 condensing enzyme for cuticular wax production in Arabidopsis. Plant Physiol. **129,** 1568–1580.

Jefferson, R.A., Kavanagh, T.A., and Bevan, M.W. (1987). GUS fusions: Beta-glucuronidase as a sensitive and versatile gene fusion marker in higher plants. EMBO J. **6,** 3901–3907.

Jeffree, C. (1996). Structure and ontogeny of plant cuticles. In Plant Cuticles: An Integrated Functional Approach., G. Kerstiens, ed (Oxford, UK: Bios Scientific Publishers), pp. 33–82.

Jenks, M.A., Joly, R.J., Peters, P.J., Rich, P.J., Axtell, J.D., and Ashworth, E.N. (1994). Chemically induced cuticle mutation affecting epidermal conductance to water vapor and disease susceptibility in *Sorghum bicolor* (L.) Moench. Plant Physiol. **105,** 1239–1245.

Jenks, M.A., Tuttle, H.A., Eigenbrode, S.D., and Feldmann, K.A. (1995). Leaf epicuticular waxes of the eceriferum mutants in Arabidopsis. Plant Physiol. **108,** 369–377.

Jeon, J.S., et al. (2000). T-DNA insertional mutagenesis for functional genomics in rice. Plant J. **22,** 561–570.

Jeong, D.H., An, S., Kang, H.G., Moon, S., Han, J.J., Park, S., Lee, H.S., An, K., and An, G. (2002). T-DNA insertional mutagenesis for activation tagging in rice. Plant Physiol. **130,** 1636–1644.

Jung, K.H., Han, M.J., Lee, Y.S., Kim, Y.W., Hwang, I., Kim, M.J., Kim, Y.K., Nahm, B.H., and An, G. (2005). Rice *Undeveloped Tapetum1* is a major regulator of early tapetum development. Plant Cell **17,** 2705–2722.

Jung, K.H., Hur, J., Ryu, C.H., Choi, Y., Chung, Y.Y., Miyao, A., Hirochika, H., and An, G. (2003). Characterization of a rice chlorophyll-deficient mutant using the T-DNA gene-trap system. Plant Cell Physiol. **44,** 463–472.

Kolattukudy, P.E. (1996). Biosynthetic pathways of cutin and waxes, and their sensitivity to environmental stresses. In Plant Cuticles: An Integrated Functional Approach., G. Kerstiens, ed (Oxford, UK: Bios Scientific Publishers), pp. 83–108.

Kumar, S., Tamura, K., Jakobsen, I.B., and Nei, M. (2001). MEGA2: Molecular evolutionary genetics analysis software. Bioinformatics **17,** 1244–1245.

Kunst, L., and Samuels, A.L. (2003). Biosynthesis and secretion of plant cuticular wax. Prog. Lipid Res. **42,** 51–80.

Lee, S., Jeon, J.-S., Jung, K.-H., and An, G. (1999). Binary vectors for efficient transformation of rice. J. Plant Biol. **42,** 310–316.

Lee, S., Jung, K.H., An, G., and Chung, Y.Y. (2004). Isolation and characterization of a rice cysteine protease gene, *OsCP1*, using T-DNA gene-trap system. Plant Mol. Biol. **54,** 755–765.

Lee, S., Kim, J., Son, J.S., Nam, J., Jeong, D.H., Lee, K., Jang, S., Yoo, J., Lee, J., Lee, D.Y., Kang, H.G., and An, G. (2003). Systematic reverse genetic screening of T-DNA tagged genes in rice for functional genomic analyses: MADS-box genes as a test case. Plant Cell Physiol. **44,** 1403–1411.

Meuter-Gerhards, A., Riegart, S., and Wiermann, R. (1999). Studies on sporopollenin biosynthesis in *Cucurbita maxima* (DUCH)-II: The involvement of aliphatic metabolism. J. Plant Physiol. **154,** 431–436.

Millar, A.A., Clemens, S., Zachgo, S., Giblin, E.M., Taylor, D.C., and Kunst, L. (1999). *CUT1*, an *Arabidopsis* gene required for cuticular wax biosynthesis and pollen fertility, encodes a very-long-chain fatty acid condensing enzyme. Plant Cell **11,** 825–838.

Nawrath, C. (2003). The biopolymers cutin and suberin. In The Arabidopsis Book, C.R. Somerville and E.M. Meyerowitz, eds (Rockville, MD: American Society of Plant Biologists), doi/10.1199/tab.0099, http://www.aspb.org/publications/arabidopsis/.

Paxson-Sowders, D.M., Dodrill, C.H., Owen, H.A., and Makaroff, C.A. (2001). DEX1, a novel plant protein, is required for exine pattern formation during pollen development in Arabidopsis. Plant Physiol. **127,** 1739–1749.

Piffanelli, P., Ross, J.H.E., and Murphy, D.J. (1997). Intra- and extracellular lipid composition and associated gene expression patterns during pollen development in *Brassica napus*. Plant J. **11,** 549–562.

Piffanelli, P., Ross, J.H.E., and Murphy, D.J. (1998). Biogenesis and function of the lipidic structures of pollen grains. Sex. Plant Reprod. **11,** 65–80.

Pighin, J.A., Zheng, H., Balakshin, L.J., Goodman, I.P., Western, T.L., Jetter, R., Kunst, L., and Samuels, A.L. (2004). Plant cuticular lipid export requires an ABC transporter. Science **306,** 702–704.

Pruitt, R.E., Vielle-Calzada, J.P., Ploense, S.E., Grossniklaus, U., and Lolle, S.J. (2000). *FIDDLEHEAD*, a gene required to suppress epidermal cell interactions in *Arabidopsis*, encodes a putative lipid biosynthetic enzyme. Proc. Natl. Acad. Sci. USA **97,** 1311–1316.

Riederer, M., and Schreiber, L. (2001). Protecting against water loss: Analysis of the barrier properties of plant cuticles. J. Exp. Bot. **52,** 2023–2032.

Schnurr, J., Shockey, J., and Browse, J. (2004). The acyl-CoA synthetase encoded by *LACS2* is essential for normal cuticle development in *Arabidopsis*. Plant Cell **16,** 629–642.

Scott, R.J. (1994). Pollen exine: The sporopollenin enigma and the physics of pattern. In Molecular and Cellular Aspects of Plant Reproduction, R.J. Scott and A.D. Stead, eds (Cambridge, UK: Cambridge University Press), pp. 49–81.

Taton, M., Husselstein, T., Benveniste, P., and Rahier, A. (2000). Role of highly conserved residues in the reaction catalyzed by recombinant Delta7-sterol-C5(6)-desaturase studied by site-directed mutagenesis. Biochemistry **39,** 701–711.

Todd, J., Post-Beittenmiller, D., and Jaworski, J.G. (1999). *KCS1* encodes a fatty acid elongase 3-ketoacyl-CoA synthase affecting wax biosynthesis in *Arabidopsis thaliana*. Plant J. **17,** 119–130.

Triglia, T., Peterson, M.G., and Kemp, D.J. (1988). A procedure for in vitro amplification of DNA segments that lie outside the boundaries of known sequences. Nucleic Acids Res. **16,** 8186.

Vioque, J., and Kolattukudy, P.E. (1997). Resolution and purification of an aldehyde-generating and an alcohol-generating fatty acyl-CoA reductase from pea leaves (*Pisum sativum* L.). Arch. Biochem. Biophys. **340,** 64–72.

Vogg, G., Fischer, S., Leide, J., Emmanuel, E., Jetter, R., Levy, A.A., and Riederer, M. (2004). Tomato fruit cuticular waxes and their effects on transpiration barrier properties: Functional characterization of a mutant deficient in a very-long-chain fatty acid beta-ketoacyl-CoA synthase. J. Exp. Bot. **55,** 1401–1410.

Wang, A., Xia, Q., Xie, W., Datla, R., and Selvaraj, G. (2003). The classical Ubisch bodies carry a sporophytically produced structural protein (RAFTIN) that is essential for pollen development. Proc. Natl. Acad. Sci. USA **100,** 14487–14492.

Wang, A., Xia, Q., Xie, W., Dumonceaux, T., Zou, J., Datla, R., and Selvaraj, G. (2002). Male gametophyte development in bread wheat (*Triticum aestivum* L.): Molecular, cellular, and biochemical analyses of a sporophytic contribution to pollen wall ontogeny. Plant J. **30,** 613–623.

Wehling, M., Kuhls, S., and Armanini, D. (1989). Volume regulation of human lymphocytes by aldosterone in isotonic media. Am. J. Physiol. **257,** E170–E174.

Welker, O.A., and Haas, K. (1998). Structure and composition of epicuticular wax in rice leaves and its eco-physiological significance. In Agroecology, Plant Protection and the Human Environment: Views and Concepts, K. Martin, J. Müther, and A. Auffarth, eds (Weikersheim, Germany: PLITS), pp. 109–117.

Wiermann, R., and Gubatz, S. (1992). Pollen wall and sporopollenin. Int. Rev. Cytol. **140,** 35–72.

Wilmesmeier, S., Steuernagel, S., and Wiermann, R. (1993). Comparative FTIR and ^{13}C CP/MAS NMR spectroscopic investigations on sporopollenin of different systematic origins. Z. Naturforsch. **48c,** 697–701.

Wilmesmeier, S., and Wiermann, R. (1995). Influence of EPTC (S-ethyl dipropyl-tricabamate) on the composition of surface waxes and sporopollenin structure in *Zea mays*. J. Plant Physiol. **146,** 22–28.

Xu, X., Dietrich, C.R., Delledonne, M., Xia, Y., Wen, T.J., Robertson, D.S., Nikolau, B.J., and Schnable, P.S. (1997). Sequence analysis of the cloned *glossy8* gene of maize suggests that it may code for a beta-ketoacyl reductase required for the biosynthesis of cuticular waxes. Plant Physiol. **115,** 501–510.

Xu, X., Dietrich, C.R., Lessire, R., Nikolau, B.J., and Schnable, P.S. (2002). The endoplasmic reticulum-associated maize GL8 protein is a component of the acyl-coenzyme A elongase involved in the production of cuticular waxes. Plant Physiol. **128,** 924–934.

Zheng, H., Rowland, O., and Kunst, L. (2005). Disruptions of the *Arabidopsis Enoyl-CoA reductase* gene reveal an essential role for very-long-chain fatty acid synthesis in cell expansion during plant morphogenesis. Plant Cell **17,** 1467–1481.